journal of the international meteor organization

# WGN

37:4
august 2009

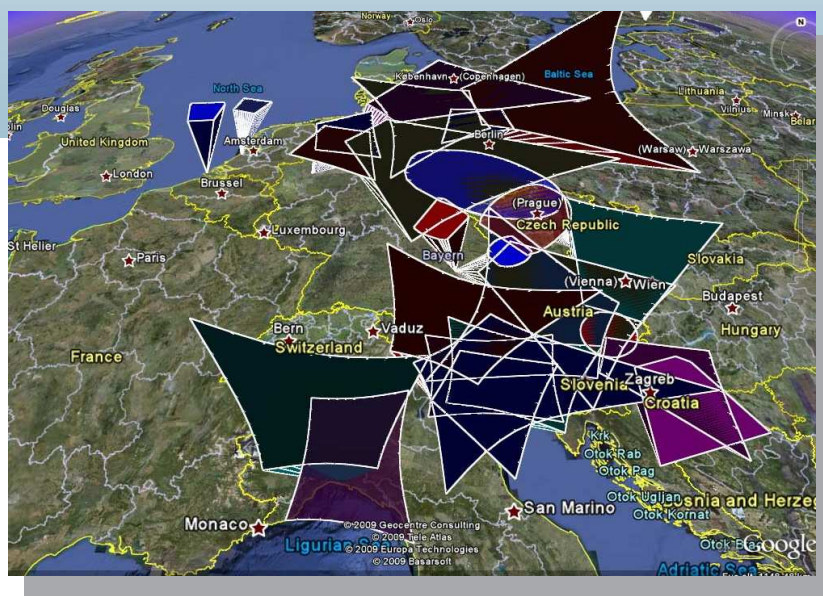


10 years of the IMO Video Meteor Network

Leonids

ISSN 1016-3115

WGN Vol. 37, No. 4, August 2009, pp. 97 – 132

## Administrative



## Ongoing meteor work



## Preliminary results



## History



## Front cover image

The area over central Europe covered by the cameras of the IMO Video Meteor Network on December 2008. For the detailed analysis of the Network data, see the article on page 98.

## Future covers

Have you an interesting or spectacular meteor photograph that you think would look good on the cover of WGN? If so, please offer it to us. A brief description will also be required: this should say what the photograph shows, when and where it was taken, plus (if possible) technical details such as the camera and exposure. We can be contacted at `wgn@imo.net`, but remember to put 'Meteor' in the subject line to get round the anti-spam filters.

## Writing for WGN

This Journal welcomes papers submitted for publication. All papers are reviewed for scientific content, and edited for English and style. Instructions for authors can be found in WGN **31:4**, 124–128, and at `http://www.imo.net/articles/writingforwgn.pdf` .

## Cover design

Rainer Arlt

## Copyright



## Legal address

International Meteor Organization, Mattheessensstraat 60, 2540 Hove, Belgium.

# Guest Editorial – 10 Years of the IMO Video Meteor Network

*Sirko Molau*

In 1992 I did my first meteor recordings by video. In the next year I started to work on a computer-based meteor detection and analysis with a cheap, custom-made framegrabber. In the beginning, the computer hardware was too slow to do everything in real-time, but right from the start I dreamt of an automated meteor camera.

Based on the experience I gained with the first software, I started to work on MetRec around 1997/98. In the beginning, the software was only able to detect meteors. I remember a discussion I had with a German visual meteor watcher after a presentation of the software at some meeting. What he had seen was not sufficient to him. He envisioned a camera that he would install at a dark side, and all he would need to do was to start the system. Then everything should be done automatically: The meteors should be detected, measured, and stored by software, that in the end he only was to collect the observing results. And I remember my reply, that this was wishful thinking: I knew that computers would support us with the analysis of video data, but a fully automated system seemed impossible to me. Still, what he had said was in fact my own dream from the early days on, and his comment remained in the back of head for many years.

In the next months, MetRec further evolved and new functions were implemented. Early 1999 I realized, that an automated system had become possible. Instead of only analysing old video tapes for testing I started to record the night sky in real time and collect meteor data in March 1999. By the end of March, I presented first results at the AKM spring meeting and it was no big deal to convince Jürgen Rendtel, a much more active meteor observer than me, to do the same with his own camera. That was the beginning of the IMO Video Meteor Network.

Also in subsequent months and years, a number new functions were added to MetRec. Many of these were inspired by the experiences we made with every-day operation of MetRec. Only a few years later we saw the first truly automated camera systems which were powered on at dusk by a time switch and shut down on the next morning. For the last three years, I have been operating myself cameras at a remote site that I visit only every other month to check the system, clean the front window and collect the data.

Now, 10 years after my first real-time observations, the IMO network has evolved to a community of observers in many different countries who record large amounts of meteor data in each clear night. How useful these data are is demonstrated by the analysis that is presented in this issue of WGN. And as the network is further growing, we will collect even more data in the future and obtain even more precise results about the major and minor meteor showers round the year.

In the beginning, there was a dream: The dream, to automatically record and analyse video meteors in large quantities. For many years I spent most of my spare time to make this dream come true (and I am still doing so these days), but it is a wonderful feeling to see that we have reached what seemed to be futuristic to me a decade ago. This is the time to earn the fruits of our work!

IMO bibcode WGN-374-editorial NASA-ADS bibcode 2009JIMO...37...97M

# Ongoing meteor work

## A Comprehensive List of Meteor Showers Obtained from 10 Years of Observations with the IMO Video Meteor Network

*Sirko Molau* [1] *and Jürgen Rendtel* [2]

We have analysed data of more than 450 000 video meteors recorded over more than 10 years in the IMO Video Network. The single station data cover all Solar longitudes and allow to derive positions of radiants and the corresponding velocities as well as activity information for meteor showers. We present results for 9 major showers, 44 minor showers and 12 new detections. Shower data are compared with the entries kept by the IAU Meteor Data Center. For some showers we find a systematic shift of the velocity during the activity period.

Received 2009 August 10

### 1 Introduction

Video meteor observations have significantly increased our knowledge about meteor showers over the recent years. Whereas first observations of amateurs with image-intensified cameras date back to the 1980s, it was the shift towards automated observation that paved the road for the breakthrough of this technique. For over ten years now, video observers from several countries have collected video meteors in the same fashion and created an unprecedended database of more than 450 000 single station video meteors to date. Starting in 2005, automated statistical analysis procedures were developed to extract reliable meteor shower information from the database. First results were presented by Molau (2006 and 2008). Earlier this years, results from the Japanese SonotaCo network were published (SonotaCo, 2009). They represent an independent data set which is analyses based on different analysis algorithms (double-station) and software (UFO* tool set). The results obtained by SonotaCo were in good agreement with our findings, which proved the maturity of our analysis technique and encouraged us to carry out a new analysis. This time, the automated shower extraction was only the first step. The results for each shower were manually checked and refined. Weak shower detections with strong scatter in radiant position or shower velocity were omitted; showers that were artificially split by the analysis software were joined. We compared the detected shower with the compilation of radiants (Jopek, 2009) in the IAU Meteor Data Center (called MDC list hereafter) and recalculated meteor shower parameters (radiant position and drift, activity interval, meteor shower velocity and activity) after rejecting outliers. The result is a comprehensive list of 65 meteor showers obtained from over ten years of observations in the IMO video network.

In this paper we first introduce the IMO Video Meteor Network, which provided the observational basis for this anaylsis. Then we describe the data set and give an outline of the analysis algorithm. We describe the analysis of selected showers in detail to demonstrate what can be achieved with the data. Thereafter, the detected meteor showers are presented and discussed. We start with nine major well-known showers to explore the limits, when their signal is strong enough to stand out of the sporadic background. Next we concentrate on minor showers, which are marked as established in the MDC list. Moving further towards the detection limit, we present minor showers from the MDC list, who have a working status but could be confirmed by our analysis. Next we list a set of new showers that were obtained from the IMO Video Meteor Database. For each shower, we give the interval of activity, radiant position and drift, meteor shower velocity, the maximum video rate (a measure of the meteor shower activity similar to the visual ZHR) as well as an activity profile. We also state, how many single station meteors from the IMO database were attributed to the meteor shower. Finally we report on short-duration showers from the MDC list, which were only detected after we relaxed the minimum meteor shower duration criterion, and finally we present and discuss those showers that are marked as established in the MDC list, but cannot be detected in our database.

In this paper, we leave out results concerning the Antihelion source (except the Taurid branches) as well as sporadic sources (e.g. Apex and Antapex source). These are frequently detected in the video data, but their analysis deserves special care, because they have large radiation areas and stronger scatter in velocity. We also note that there is a complex of radiants in Perseus and Auriga in September/October, which needs special treatment to identify the individual branches. All of these will be subject of aditional analyses presented in the future.

Throughout the paper, we use the MDC numbers and three-letter codes for the showers. For convenience, we also give the shower designations in the respective sections.

### 2 The IMO Video Meteor Network

The continuous monitoring of the night sky by video meteor cameras started with a first station in Aachen (Germany) in March 1999 (Molau, 2001). Other ob-

[1]Abenstalstr. 13b, 84072 Seysdorf, Germany.
Email: sirko@molau.de
[2]Eschenweg 16, 14476 Marquardt, Germany.
Email: jrendtel@aip.de

IMO bibcode WGN-374-molau-videoshowers
NASA-ADS bibcode 2009JIMO...37...98M

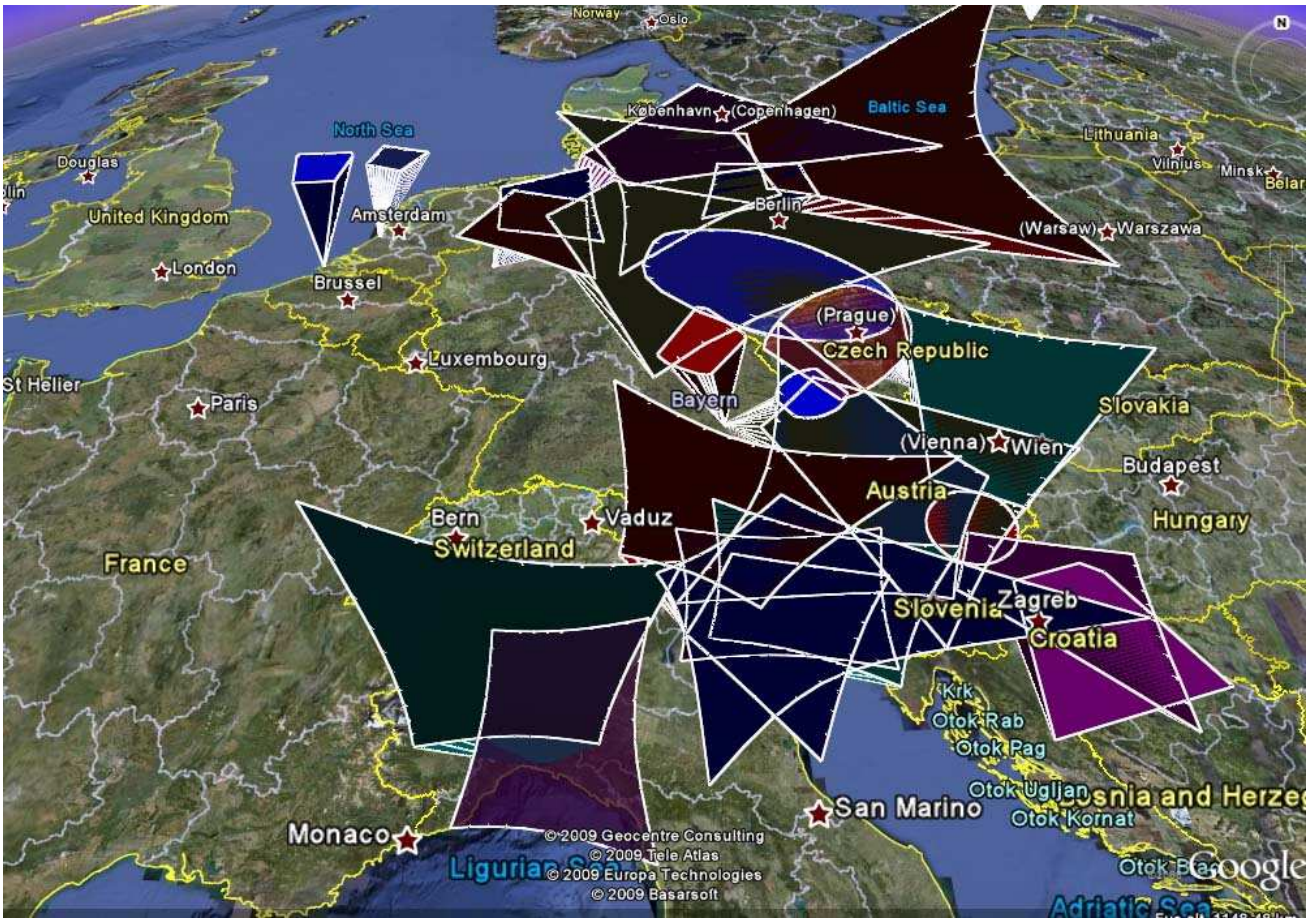


*Figure 1* – Fields of view of the IMO network cameras in Central Europe as of December 2008.

servers joined the AKM network (Arbeitskreis Meteore, AKM), and by the end of 1999, five German observers had collected over 8 000 meteors within 1 000 hours of effective observing time. In the following years, the network grew steadily, and by 2004 it was renamed to IMO Video Meteor Network because of its international character.

The common characteristic of all observers in the IMO network is the use of the MetRec software (Molau, 1998). The PAL/NTSC signal of the video camera is directly fed into the analysis PC, digitized with a Matrox Meteor II framegrabber, and inspected by the MetRec software in real-time. Once a meteor is detected, astrometric and photometric routines are applied. The position, brightness and velocity of each meteor are stored together with a sum image and a short time-sequence of the event. All observers send their data on a monthly basis to the IMO video commission, where they are quality-checked, corrected if necessary, analyzed, archived and published.

Right from the start, the IMO Network focused on single station observation. The major advantage is, that each observer with the right equipment can participate in the network and provide useful data, no matter how many cameras there are in his part of the world. There is no need to synchronize the fields of view and technical parameters of individual cameras for double station work. Each meteor contributes to the analysis independently where and when it was observed, whether there are other recordings from the same event or how the observing geometry looks like. On the other hand, meteor trajectories and orbits cannot be determined directly from single station data. It requires large data sets and sophisticated statistical algorithms to reveal not only the radiant position of meteor showers, but also their pre-atmospheric entry velocity, the interval of activity and activity profiles with high precision.

Two types of video cameras are most popular these days. On the one hand, there are non-intensified Mintron and Watec cameras with Sony ExView HAD chip as sensor, typically equipped with $f/0.8$ Computar c-mount lenses of 3.8, 6, or 8 mm focal length. Their field of view ranges between 40 and 80° with limiting magnitudes between +3 and +4 mag. On the other hand, there are a few image-intensified cameras. Most popular is the Philips XX-1332 second generation image intensifier tube (or other brands of the same device) with 50 mm photo cathode. In connection with a $f =$ 50 mm $f/1.4$ standard photographic lens, it achieves a field of view of roughly 60° at limiting magnitudes beyond +6 mag. Under dark skies, image-intensified cameras record on average about a factor of three more meteors than non-intensified cameras, but they are more delicate and therefore difficult to handle in automated systems.

Over the years, the degree of automation has increased significantly in the IMO network. In the beginning, the cameras were manually started in clear nights. Nowadays, most cameras are operated fully automated. They are activated by a time switch in the evening and

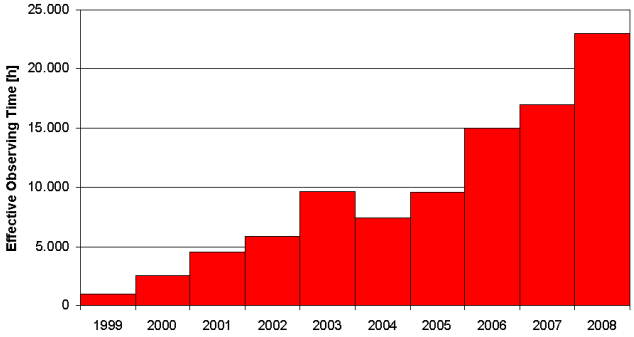


*Figure 2* – Effective observing time of the IMO Video Meteor Network 1999–2008.

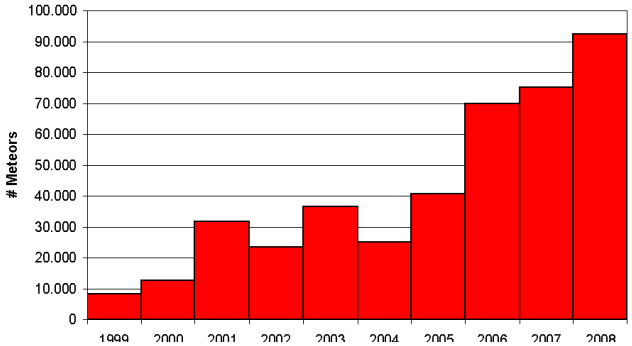


*Figure 3* – Number of meteors recorded by the IMO Video Meteor Network 1999–2008.

shut down automatically in the morning. Thus, they cover meteor activity at any time with clear skies. Also the size of the network has extended significantly over the last ten years. Most parts of Central Europe are well covered (Figure 1), and two cameras are operated in North America.

Thanks to the network size and the high degree of automation, the amount of data and their quality have increased significantly over the recent years. In 2008, 24 observers from ten countries contributed to the network with overall 37 cameras (Molau & Kac, 2009). They recorded more than ten times as many meteors within twenty times as many observing hours than in 1999. Between 2006 and 2008, there was just a single night without a meteor record because of poor weather at all sites. Figure 2 shows the total effective observing time in the IMO Video Meteor Network, and Figure 3 the number of meteors recorded each year. Until mid-2009, more than 30 observers from twelve countries (Australia, Czech Republic, Finland, Germany, Hungary, Italy, Portugal, Slovenia, Spain, the Netherlands, UK, and the USA) submitted their data.

## 3 Data set and analysis procedure

The analysis presented here is based on all data collected by the IMO network until June 2009. Thus, beside the main data set 1999–2008, also roughly 5 000 meteors recorded before the start of the network (1993–1998) and 31 000 meteors from the first half of 2009 were included. The resulting data set consists of 451 282 single station meteors recorded in 3 363 observing nights and 107 594 hours of effective observing time. Table 1

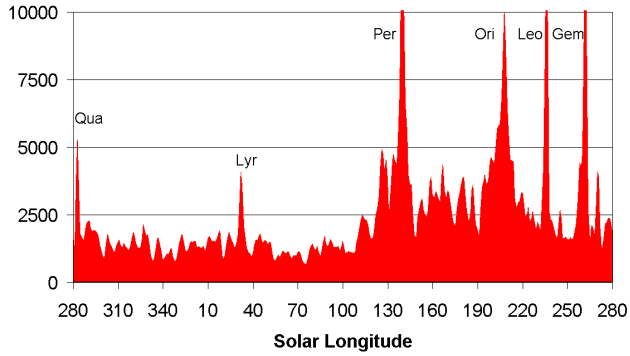


*Figure 4* – Distribution of meteors over Solar longitude. Due to overlapping sliding intervals, each meteor contributes twice.

gives an overview of all observers contributing more than ten observing nights to the video database. We are grateful to their passion, which enabled the collection of this to-date unprecedented data set of high-quality meteor recordings in the optical domain, completely covering all solar longitudes.

Figure 4 depicts the distribution of meteors over Solar longitude. The analysis was based on sliding intervals of two degrees length and one degree shift, so each meteor contributed to two consecutive solar longitude intervals. The times of the major showers with up to 16 000 meteors per interval are clearly visible. But also times of low meteor shower activity are well covered – there is no single interval with less than 680 meteor records. The average is close to 2 500 meteors per interval.

The procedure used to analyze this data set has been applied first to a smaller subset in 2006 (Molau, 2006). It was refined in a second analysis (Molau, 2008). Here we give a short summary of the algorithms.

For each meteor, the time and place of observation as well as the coordinates of the start and end point and the angular velocity are given. Meteor shower radiants are described by four parameters: their position (right ascension $\alpha$ and declination $\delta$), velocity at infinity $V_\infty$, and the Solar longitude $\lambda_\odot$. For each pair of meteor $m$ and radiant $r$, a conditional probability $P(m|r)$ can be calculated. It describes the probability, that the meteor belongs to the (zenith attraction corrected) radiant. The conditional probability is computed from two measures – the distance $d$ (in °) at which the backward prolongation of the meteor misses the radiant, and the difference $v$ (in °/s) between the expected and the observed angular meteor velocity. The expected angular velocity that a meteor from radiant $r$ would have at the position of $m$, is calculated on the basis of the average meteor altitude, which was recently refined (Molau & SonotaCo, 2009). Both the radiant miss distance and the angular velocity difference are combined in a three-dimensional Laplacian probability distribution. The type of distribution and its parameters were obtained from data (Molau, 2008) and reflect typical video observation errors:

*Table 1* – Observers who contributed more than 10 observing nights to the IMO Video Meteor Network.

| Observer | Country | IMO Code | Nights | Eff. obs. time [h] | Meteors |
|---|---|---|---|---|---|
| Sirko Molau | DE | MOLSI | 2344 | 20 807.2 | 127 072 |
| Jörg Strunk | DE | STRJO | 1696 | 12 709.4 | 42 009 |
| Javor Kac | SL | KACJA | 1173 | 10 333.0 | 31 354 |
| Ilkka Yrjölä | FI | YRJIL | 942 | 5 419.2 | 18 596 |
| Stane Slavec | SL | SLAST | 871 | 4 318.9 | 11 262 |
| Flavio Castellani | IT | CASFL | 794 | 5 775.4 | 13 802 |
| Orlando Benitez-Sanchez | ES | BENOR | 733 | 4 088.3 | 10 473 |
| Jürgen Rendtel | DE | RENJU | 647 | 3 823.4 | 17 223 |
| Bernd Brinkmann | DE | BRIBE | 598 | 2 376.2 | 8 366 |
| Detlef Koschny | NL | KOSDE | 509 | 3 126.3 | 11 567 |
| Mihaela Triglav | SL | TRIMI | 505 | 2 585.9 | 8 474 |
| Robert Lunsford | US | LUNRO | 495 | 3 204.2 | 22 122 |
| Enrico Stomeo | IT | STOEN | 492 | 3 605.5 | 13 854 |
| Stephen Evans | UK | EVAST | 457 | 2 807.3 | 11 411 |
| Wolfgang Hinz | DE | HINWO | 455 | 2 689.5 | 13 690 |
| Carl Hergenrother | US | HERCA | 399 | 2 805.7 | 5 570 |
| Steve Quirk | AU | QUIST | 341 | 3 041.8 | 10 109 |
| Rui Goncalves | PT | GONRU | 320 | 2 850.6 | 9 931 |
| Stefano Crivello | IT | CRIST | 229 | 1 459.4 | 6 217 |
| Biondani Roberto | IT | ROBBI | 229 | 1 261.6 | 4 082 |
| Mirko Nitschke | DE | NITMI | 213 | 942.5 | 5 425 |
| David Przewozny | DE | PRZDA | 196 | 1 073.6 | 3 745 |
| Stefan Ueberschaer | DE | UEBST | 173 | 882.3 | 1 684 |
| Maurizio Eltri | IT | ELTMA | 169 | 1 210.4 | 5 886 |
| Ulrich Sperberg | DE | SPEUL | 159 | 1 021.6 | 4 339 |
| Paolo Ochner | IT | OCHPA | 134 | 733.2 | 1 763 |
| Rosta Stork | CZ | STORO | 98 | 1 052.8 | 14 732 |
| Rob McNaught | AU | MCNRO | 52 | 401.2 | 5 285 |
| Andre Knöfel | DE | KNOAN | 47 | 289.0 | 648 |
| Klaas Jobse | NL | JOBKL | 47 | 288.0 | 2 231 |
| Mitja Govedič | SL | GOVMI | 33 | 156.7 | 489 |
| Antal Igaz | HU | IGAAN | 32 | 217.7 | 369 |
| Miloš Weber | CZ | WEBMI | 29 | 49.4 | 1 050 |
| other | | | 25 | 186.8 | 6 452 |
| Overall | | | 3363 | 107 594.0 | 451 282 |

$$P(m|r) = \exp(-0.8 \times d) \times \exp\left(\frac{-v}{0.4 + v/50}\right).$$

Based on the conditional probability, a search for possible meteor shower radiants is carried out, which is the computationally most demanding part of the analysis. At first the data set is cut into Solar longitude slices (two degrees length, one degree shift). For each Solar longitude interval, an iterative search procedure is carried out.

At initialization, the probability of each possible radiant point (position in steps of 0.°5, velocity at infinitiy in steps of 1 km/s) is accumulated over all meteors of the interval. The probability distributions of individual meteors are not normalized, i.e. the most probable radiant gets a value of 1.0 and the probability mass provided by each meteor differs. In the iterative phase, the radiant with highest accumulated probability is selected. According to standard criteria for meteor shower assignment, all meteors belonging to that radiant are determined and taken out of the data set. Their probability distribution is calculated and subtracted from the overall distribution. Then the next iteration is carried out to extract the next strongest radiant. The procedure terminates after 50 iterations. To avoid interference of nearby radiants, the meteor shower assignment is repeated once all radiants are determined (Molau, 2008).

After the most probable radiants are determined for each solar longitude, similar radiants in consecutive Solar longitude intervals are connected to identify meteor showers. The showers are compared against the current MDC list (Jopek, 2009) to classify known showers. The main parameters that determine the number and quality of detected meteors showers are the minimum number of intervals with suitable radiants (minimum meteor shower duration: 5° in Solar longitude), the maximum position difference (7°) and the maximum velocity difference (7 km/s) between the radiants from one Solar longitude interval to the next. In brackets are the figures use primarily for this analysis.

Once the meteor showers were determined, their basic parameters (activity interval and date of maximum activity, radiant position and drift, average velocity) were calculated. To compute the meteor shower activity is in particular challenging, as the data set was a mixture of observations from different cameras with different lenses under different observing conditions. Neither the effective observing time nor the field of view nor limiting magnitude per Solar longitude were known. At first, the observation probability (Molau, 2008) was applied to each meteor that belongs to a detected radiant. This probability is the average of the sine of the radiant altitude at night time in the given solar longitude interval. A meteor from a hypothetical radiant that is all night long at zenith would get a weight of 1.0, whereas a meteor from a radiant that is visible for only a short time near the horizon would get a weight of up to 100. This way, the geometric observing conditions are corrected – typical observability function weights at mid-northern latitude range between 1.5 for easily visible Geminids and 30 for the difficult to observe $\eta$-Aquariids.

In the next step, all meteors that belong to showers are counted, and all remaining meteors are declared as sporadics. The meteor shower activity (called video rate VR hereafter) at a certain Solar longitude is now the ratio between the observability function corrected number of shower meteors and the number of sporadics in that interval. This way, the difference in effective observing time, field of view diameter and limiting magnitude is accounted for.

Finally, the video rate is scaled and corrected for the annual sporadic activity variation. It was found that the sporadic activity in the Northern hemisphere can be approximated by a sine shaped function with a minimum of 2.2 meteors per hour at Solar longitude 350° and a maximum of 4.2 at 170° (Molau, 2008). The scaling factor was initally chosen such that the $\eta$-Aquariids yield a maximum VR of 50. It turned out, that the video rate VR resembles the long-term ZHR of a shower remarkably well. Thus, we are confident that we can not only give a qualitative account of meteor shower activity (shape of the activity profile and time of the maximum), but also a quantitative estimate of the ZHR. Due to the 2-day-intervals, however, the peaks are significantly smoothed out and therefore below the peak ZHRs derived from short intervals.

## 4 Manual refinement

All automatically detected showers were manually checked. When the video rate of a shower falls below one, the sporadic dilution becomes dominating. For this reason, there are typically a few uncertain intervals at the begin and end of each shower activity period, which are affected by chance alignments with sporadic meteors. We reduced the activity intervals of each shower to those with radiant position and velocity fitting well to the average shower parameters. We corrected cases, where one shower was cut into two, and we omitted showers, which contained only few meteors and showed strong scatter from one solar longitude interval to the next.

To account for meteor showers of shorter duration, we repeated the meteor shower search with reduced minimum meteor shower duration of four and three degrees in Solar longitude. Naturally, the number of possible showers grew significantly, so we focused on those which were not found in the previous analysis with longer duration, and which fitted well to showers from the MDC list.

In the next steps, the meteor shower parameters were refined. The position and drift of the radiant was re-calculated in the possibly reduced Solar longitude interval by a weighted linear regression, with the absolute meteor counts per interval taken as weight. For major showers, the Solar longitude of the maximum activity was re-calculated as the weighted mean Solar longitude, using only the intervals of highest activity with the video rate as weight. The meteor shower velocity was refined as well. It is the average over all Solar

longitude intervals. Here, each value was weighted by the meteor number. This allows us to report both the Solar longitude (i.e. date) of the shower maximum and the velocity rounded to the nearest 0.1 degree or km/s, respectively, even though the underlying analysis was carried out for steps of 1 degree in solar longitude and 1 km/s in velocity $V_\infty$.

We estimate that the accuracy of the radiant position is better than 1° if the activity VR $\geq$ 2, and the average velocity at infinity is accurate to 1 km/s for all showers.

## 5 Meteor shower velocities

When calculating the radiant position and drift for long duration meteor showers, we noted that in some cases the meteor shower velocity did not only show some arbitrary scatter around the average value, but that the calculated velocity increased or decreased systematically over the activity period. At first we did not pay special attention to this observation, because we assumed that to be an artefact of the analysis procedure. However, on our request, the Japanese meteor observer SonotaCo checked his data set of meteoroid orbits obtained from the SonotaCo video network (SonotaCo, 2009) and found similar variations. Even more, for all four showers which have been compared in detail (ETA, PER, SDA and ORI), he reported exactly the same behaviour (decreasing, constant or increasig velocity) with only little deviation in the amount of the velocity change.

As both data sets and analysis procedures are completely independent, we conclude that the observed variations in meteor shower velocity over time are real. For this reason, we add the detected variation in velocity (in km/s per degree in Solar longitude) for all major and long-lasting showers with sufficient data. We found that LYR, ETA, and KCG are showers with a particularly large increase in velocity over time, whereas SDA, QUA, CAP, NOO and JPE show considerable velocity decreases.

As the Earth crosses different sections of the meteoroid stream over a longer period which have undergone numerous and variable orbit perturbations, these variations need to be correlated with the Earth-meteoroid collision geometry. For example, we find that the shift is in the opposite direction for the Orionids and the $\eta$-Aquariids, and larger in the latter case. As the showers represent different cross-sections through the same meteoroid stream with the Orionids being the far more distant path from the centre, the numbers listed in Table 2 indicate that this effect may also be related to different ejection speeds from the parent comet. However, at this time we have no proven explanation for the observed velocity changes.

## 6 Application of the method and results of radiant searches

First of all, our data provides us with a detailed set of information about all major showers, such as their activity period and their radiant position and drift. The

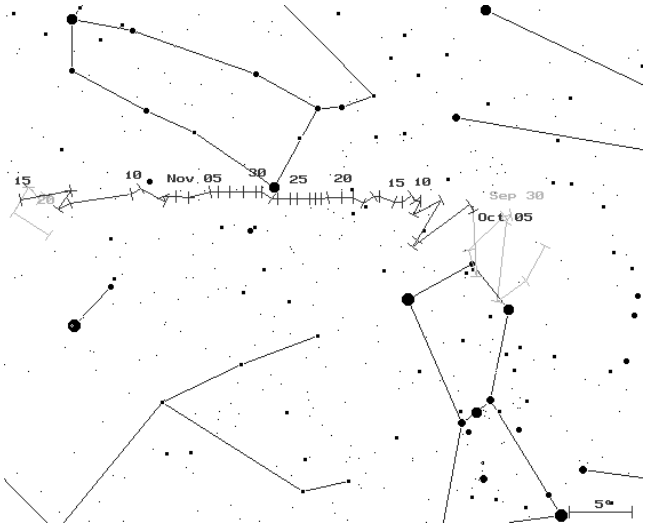


*Figure 5* – Radiant of the Orionids derived from the video data. The shaded (grey) parts at the outer edges of the drift path show the position found from the data which were excluded because of the position uncertainties.

MDC list distinguishes between showers that are established and those which have a working list status, labelled 'e' and 'w', respectively. The Toroidal, Apex and Antihelion sources also occur in our data set. In this paper, we concentrate on showers which are linked to neither of these permanent sporadic and ecliptical soures (except the Northern and Southern Taurids), because the analysis method was adjusted for showers with compact radiants. Sources with diffuse radiation areas would need to be treated in a different way in an extra paper. Another complex which we found deserves a detailed separate analysis is the set of showers radiating from the Perseus-Auriga region from end-August to mid-October. Of these showers, we only list the Aurigids and the September $\varepsilon$-Perseids here.

### 6.1 Major showers

The nine meteor showers with the highest activity level have been used for testing and calibrating the detectability of radiants from the data sample. We present details for the Orionids and the Quadrantids, because our results extend beyond the confirmation of their radiant position and drift and their activity level. In both cases, our data indicate a longer period in which the activity and the radiant can be clearly detected. Our activity profiles are from data collected over about a decade and for the search algorithm we also bin over an interval length of 2° in Solar longitude. For these reasons, our profiles are smoother than the graphs calculated from short binning intervals, and the peak level of the VR remains well below the peak ZHRs listed for the showers.

The **Orionids** can be observed from both hemispheres. The date of the peak as well as the radiant position and drift found from our data agree perfectly with the data stored in the MDC list. When we look at the outer edges of the shower activity, we find that the radiant can be continuously followed towards earlier and later Solar longitudes (Figure 5). Both the video

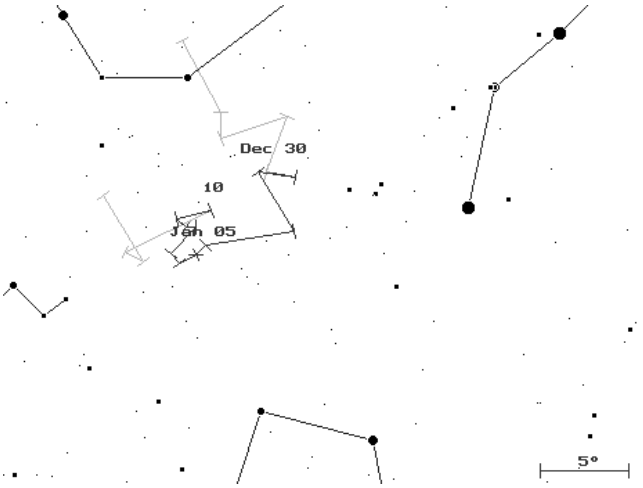


*Figure 6* – Radiant of the Quadrantids derived from the video data. In this case the position becomes uncertain in the outer bins.

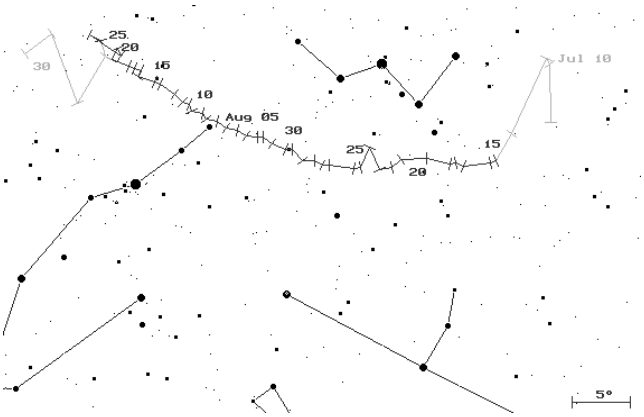


*Figure 7* – Radiant of the Perseids derived from the video data. Towards the ends, the radiant position becomes unreliable.

rate VR (shown in Figure 8) and the steady shift of the radiant position in combination with the same velocity of the meteoroids leads to an activity period which extends from end-September to November. Both parameters limit the detectability of the activity from a radiant.

Our video *rate calibration* is based on the $\eta$-Aquariids. The comparison between the VR and the long-term ZHR allows us to set a detection limit of VR = 0.7. The other limit is the reliability of the radiant position. The lower the number of true shower meteors is, the larger is the amount of sporadic meteors accidentially lining up with the radiant (and fitting the velocity). As a result of the sporadic effect, the calculated position will become uncertain and the radiant deviates from the position calculated for the neighbouring bin as shown for the Orionids in Figure 5. If these differences exceed 3° in neighbouring bins, we do not regard this as the signal of a detectable shower. These limits have been generally applied to all detections later. **Conclusion:** the detection of showers from the current data sample is possible if VR $\geq$ 0.7 and $(\Delta\alpha, \Delta\delta) \leq 3°$ per 1° in Solar longitude.

The **Quadrantids** show peak rates which are among the strongest of all showers currently observable from the Earth. Usually, the shower activity is assumed to start on January 1 and to cease by January 6. Again, our analysis shows a perfect agreement in the complete data set for the near-peak period. Moreover, the activity obviously extends in both directions. We detect meteors from the region associated to the Quadrantids from $\lambda_\odot$=274° (December 27) to 292° (January 12) with VR $>$ 0.9 all the time. As shown in Figure 6, the recorded meteors do not define a reliable radiant before 281° and after 290°. Hence we give the Quadrantid activity period as $\lambda_\odot = 281° - 290°$, here limited by the consistency of the radiant drift, although the *averaged drift* after 290° is still consistent with the period before this date. Whether the radiant becomes diffuse or this is just an effect of the small sample, cannot be decided from our analysis method.

The complete list of data obtained from the most active showers are summarized in Table 2 and compared with the MDC list entries. Graphs representing the activity in terms of VR are shown in Figure 8.

**6 LYR (Lyrids):** we find VR $\geq$ 0.6 for the entire period 24–36°; the radiant drift becomes inconsistent only in the first and last bins – hence the period of detectability is limited to 26–35°. In this interval, the VR is $\geq$ 0.7 (Figure 8).

**31 ETA ($\eta$-Aquariids):** the relative rate is VR $\geq$ 4.0 between 36 and 61°. Rather few ETA meteors have been recorded after May 18 (57°) obviously due to the shorter observing window at most observing locations. Hence the radiant position starts to become inconsistent particularly after $\lambda_\odot = 61°$ while it gives a smooth drift for the entire period before this date. Our data defines the shower over the interval $38 - 60°$. The peak rate was earlier used for calibrating the VR, hence, consistently, we find a maximum VR $\approx$ 54 (Figure 8). The velocity shift of 0.12 km/s per 1° in Solar longitude over the cross-section of the stream has been discussed in Section 5. The shift during the ETA activity is larger than in the Orionid period. The ETA meteoroids are closer to the parent's orbit and thus perhaps represent a larger variation in the ejection conditions from the inner to the outer regions of the stream.

**7 PER (Perseids):** we find VR $>$ 4 even towards August 30, but the radiant position calculated from the video data varies after August 26 (Figure 7). From the radiant data, we can trace the shower over the period 110–153° (July 13–August 26). In this case the variations of the derived radiant position in consecutive bins exceed the threshold set for a reliable shower identification while the VR would be still well above the limit. The large number of Perseids essentially in all bins also causes additional detections in the vicinity of the Perseid radiant fitting velocity and radiant drifts similar to that of the major shower. In all these cases, these virtual radiants show very large scatter in their coordinates from one bin to the next (typically more than 3°) being not parallel to the ecliptic, indicating that these are artefacts. Similar effects need to be carefully checked if detections during other major showers occur.

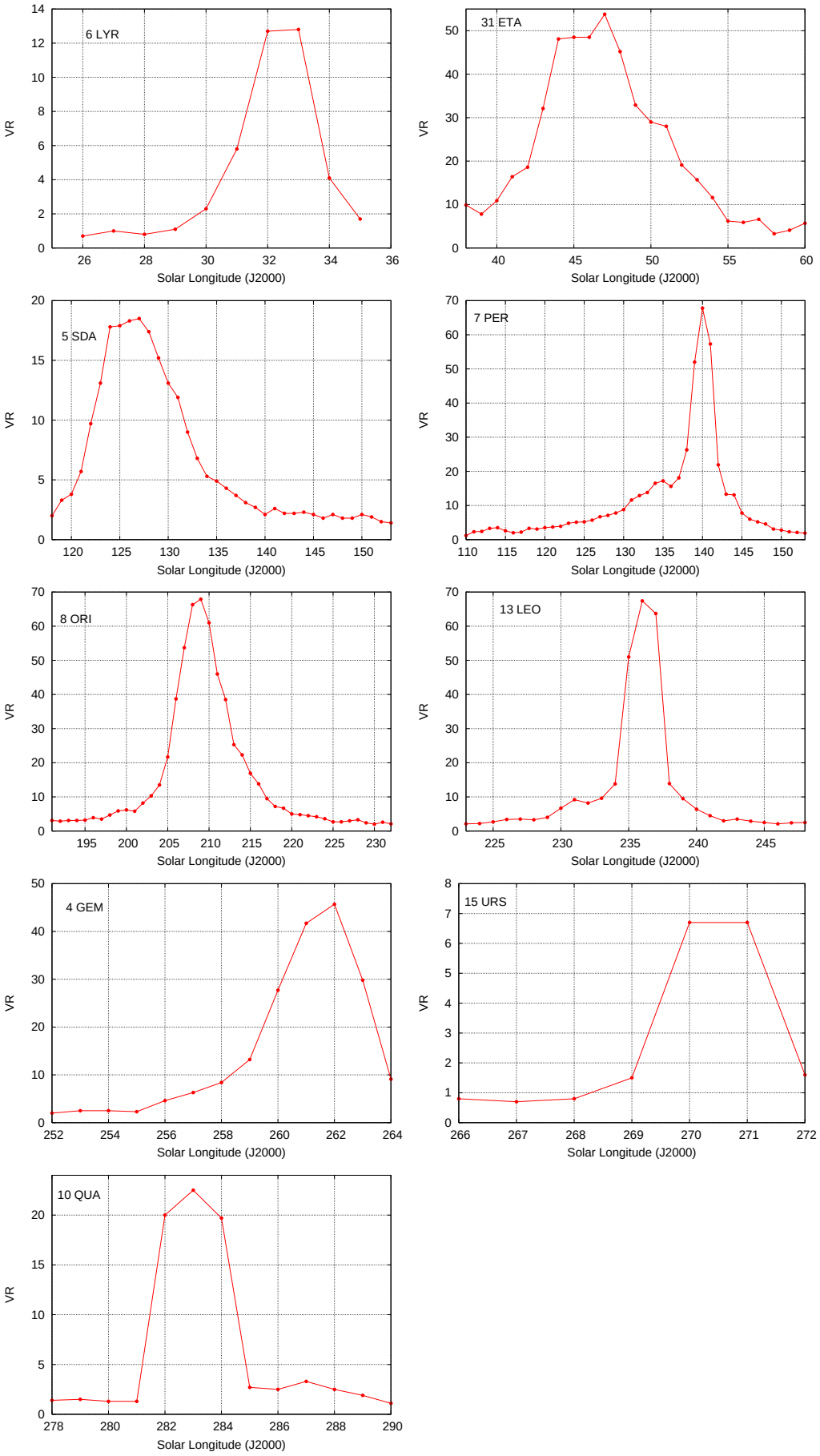


*Figure 8* – Activity profiles for the major showers derived from our video data sorted by the Solar longitude of their occurrence (same as in Table 2).

*Table 2* – Data of the major meteor showers sorted by Solar longitude (J2000.0). (V) refers to the obtained video data, (L) gives the values of the MDC list. $\Delta V_\infty$ is the observed average velocity drift over the activity period in km/s per 1° in Solar longitude. Data Met. is the number of meteors from the shower in the video database

| Shower | Peak $\lambda_\odot$[°] | | Period $\lambda_\odot$[°] | | Radiant position and drift [°] | | | | $V_\infty$ [km/s] and $\Delta V_\infty$ | | | Max. | Data |
|---|---|---|---|---|---|---|---|---|---|---|---|---|---|
| | (V) | (L) | (V) | (L) | $\alpha$ | $\Delta\alpha$ | $\delta$ | $\Delta\delta$ | (V) | | (L) | VR | Met. |
| 6 LYR | 32.4 | 32 | 26– 35 | 26– 35 | 272.2 | +0.57 | +32.9 | −0.43 | 46.2 | +0.18 | 48.4 | 13 | 1516 |
| 31 ETA | 46.8 | 46 | 38– 60 | 29– 67 | 338.9 | +0.67 | − 0.6 | +0.32 | 66.8 | +0.12 | 66.9 | 54 | 1051 |
| 5 SDA | 126.9 | 125 | 118–150 | 110–146 | 340.4 | +0.86 | −16.4 | +0.28 | 43.6 | −0.26 | 42.0 | 19 | 4716 |
| 7 PER | 140.0 | 140 | 111–153 | 114–151 | 48.1 | +1.44 | +57.6 | +0.25 | 59.0 | 0 | 60.5 | 68 | 22169 |
| 8 ORI | 208.9 | 208 | 191–232 | 189–224 | 96.1 | +0.78 | +15.5 | +0.03 | 67.3 | −0.06 | 67.1 | 68 | 18249 |
| 13 LEO | 236.1 | 235 | 223–248 | 227–241 | 154.2 | +0.61 | +21.6 | −0.29 | 70.6 | 0 | 71.5 | 67 | 9874 |
| 4 GEM | 261.5 | 262 | 252–265 | 255–265 | 113.3 | +0.96 | +32.2 | −0.17 | 35.0 | 0 | 36.4 | 46 | 13193 |
| 15 URS | 270.5 | 271 | 266–272 | 265–274 | 217.6 | +1.60 | +74.8 | −0.13 | 32.6 | – | 34.8 | 7 | 1100 |
| 10 QUA | 283.0 | 283 | 281–290 | – | 229.6 | +0.59 | +49.5 | −0.08 | 42.2 | −0.23 | 42.9 | 23 | 3184 |

*Table 3* – Data of the established minor meteor showers sorted by Solar longitude (J2000.0); V and L refer to the values obtained from this video data analysis and taken from the MDC list, respectively. If no activity period is in the list, we type '–' in the respective column. The 32 DLM shower is listed here because of its connection to the 20 COM discussed in the text. $\Delta V_\infty$ is the observed average velocity drift over the activity period in km/s per 1° in Solar longitude. 0 indicates that no drift was observed, while '–' means that no drift can be derived because of too short duration or large scatter of data points.

| Shower | Peak $\lambda_\odot$[°] | | Period $\lambda_\odot$[°] | | Radiant position and drift [°] | | | | $V_\infty$ [km/s] and $\Delta V_\infty$ | | | Max. | Data |
|---|---|---|---|---|---|---|---|---|---|---|---|---|---|
| | (V) | (L) | (V) | (L) | $\alpha$ | $\Delta\alpha$ | $\delta$ | $\Delta\delta$ | (V) | | (L) | VR | Met. |
| 145 ELY | 50 | 49 | 46– 53 | 42– 51 | 291.1 | +0.2 | +43.2 | −0.0 | 43.4 | – | 46.7 | 2.8 | 330 |
| 1 CAP | 125 | 127 | 109–138 | 101–142 | 305.1 | +0.57 | −10.2 | +0.27 | 23.7 | −0.18 | 24.9 | 5.2 | 2283 |
| 191 ERI | 137 | 137 | 132–146 | – | 43.2 | +0.8 | −11.0 | +0.4 | 64.1 | – | 65 | 4.9 | 513 |
| 12 KCG | 141 | 145 | 134–146 | 131–152 | 285.9 | +0.6 | +51.0 | +0.7 | 22.7 | +0.22 | 26.5 | 1.5 | 864 |
| 206 AUR | 158 | 158 | 156–162 | 152–165 | 90.7 | +1.5 | +39.3 | −0.4 | 66.7 | – | 67 | 3.1 | 392 |
| 208 SPE | 167 | 170 | 161–171 | 162–174 | 47.2 | +0.7 | +40.5 | +0.0 | 66.4 | – | 65.5 | 2.6 | 1118 |
| 17 NTA | 231 | 224 | 206–258 | – | 59.7 | +0.84 | +22.7 | +0.15 | 28.5 | −0.09 | 30.4 | 4.1 | 3946 |
| 2 STA | 197 | 224 | 165–237 | – | 31.7 | +0.85 | + 8.7 | +0.18 | 28.9 | −0.05 | 30.4 | 5.7 | 8355 |
| 22 LMI | 210 | 209 | 203–214 | 205–213 | 160.8 | +1.1 | +36.4 | −0.2 | 59.8 | 0 | 62.9 | 4.2 | 550 |
| 18 AND | 230 | 231 | 223–248 | – | 22.8 | +0.2 | +31.4 | +0.86 | 17.8 | 0 | 20.5 | 0.9 | 764 |
| 250 NOO | 248 | 245 | 230–254 | – | 91.9 | +0.73 | +15.2 | −0.03 | 44.1 | −0.22 | 45.1 | 3.2 | 1219 |
| 16 HYD | 254 | 265 | 244–269 | 251–273 | 123.9 | +0.80 | + 2.8 | −0.20 | 60.8 | −0.11 | 59.1 | 4.4 | 1748 |
| 19 MON | 256 | 260 | 255–268 | 245–265 | 99.2 | +0.66 | + 8.1 | −0.15 | 40.9 | 0 | 43.5 | 2.3 | 664 |
| 20 COM | 264 | 268 | 260–271 | – | 174.5 | +0.65 | +18.2 | −0.08 | 67.7 | – | 64.7 | 2.4 | 435 |
| 32 DLM | 268 | 274 | 253–315 | – | 161.5 | +0.86 | +30.5 | −0.43 | 64.0 | 0 | 63.3 | 4.4 | 3181 |
| 319 JLE | 281 | 283 | 280–285 | – | 146.6 | +0.6 | +24.4 | −0.15 | 59.2 | – | 53.9 | 0.6 | 119 |
| 331 AHY | 280 | 286 | 279–289 | – | 125.9 | +0.6 | − 7.9 | −0.14 | 43.4 | – | 45.0 | 1.5 | 187 |

**5 SDA (Southern $\delta$-Aquariids):** this is one of the few strong southern showers with a symmetric maximum (VR = 19 at $\lambda_\odot = 127°$. We find a very long 'tail' of activity, but from 156°(August 30) onwards, the radiant position becomes very uncertain with large scatter. Additionally, VR < 2.0 after $\lambda_\odot = 150°$.

**8 ORI (Orionids):** the surprisingly high peak rate of VR = 68 is mainly caused by the strong returns in the years 2006 to 2008, which make up for more than half of the overall data set. Contrary to the short peak of the Perseids, the Orionid maximum is much wider. As a result, the VR-profile suggests a shower similar in strength to the Perseids. We find VR > 2 already from 183° (September 26), but the radiant position is quite variable until 190° (October 3). At 232° (November 15) we find VR < 2 and again a variable radiant position in consecutive bins (see the remarks earlier in this Section).

**13 LEO (Leonids):** VR > 2 for the entire period, and the radiant deviates from the smooth drift only for the last bin (249°). The varying positions of Leonid peaks and storms over the entire decade cause a relatively wide maximum although each of the individual peaks lasted only for about an hour or so. In total, we can clearly detect Leonids in the period $\lambda_\odot = 223 - 248°$ (November 6–30). We find a further detection in the automatic analysis, yielding a radiant near $\vartheta$ Leonis at $\alpha = 166\overset{\circ}{.}0, \delta = 14\overset{\circ}{.}4$ with $V_\infty = 71$ km/s at $\lambda_\odot = 253°$ (December 5) which exactly fits the extrapolated Leonid drift. This apparent 'appendix' of the Leonids can be traced over eight bins (251°–258°) with a well detectable VR between 1.3 and 2.8. Perhaps the Leonids extend further than usually expected.

**4 GEM (Geminids):** this strong shower has a rather short activity period with a steep descending branch after the peak at $\lambda_\odot = 261\overset{\circ}{.}5$. We find VR ≥ 2.0 for 242–264°, i.e. December 4–16. Two bins at either sides still allow to trace the radiant, but the number of shower meteors becomes very small.

**15 URS (Ursids):** activity is detectable in the interval $\lambda_\odot = 266° - 272°$. Outside this interval, VR is < 0.7 (0.6 in the two preceeding bins, 0.4 in the two consecutive bins). Due to the unique position, the radiant is clear and consistent over the period 266–272°.

**10 QUA (Quadrantids):** we find VR ≥ 0.9 in the entire interval $\lambda_\odot = 274 - 292°$, but similar to the Orionids and as discussed above, the data yield a consistent radiant over the period $\lambda_\odot = 281 - 290°$. The narrow peak occured at slightly different positions over the decade and therefore the high rate occurs in more than one Solar longitude interval (Figure 8). Furthermore, the rate 'tail' after the peak lasts for another four bins to 288° with VR ≥ 2.5 and thus more than three times the detection threshold. Visual data yield ZHR ≥ 5 for 281°–286° and thus also a longer tailing activity than preceeding the maximum (Rendtel & Arlt, 2009; pp. 126–128).

## 6.2 Established minor showers

The analysis should also allow to detect meteor showers of low activity. First, we look at the 'established minor showers'. Of course, the category does not say anything about the strength of the source as compared to the other showers in the MDC list. The automatic analysing procedure indeed provides us with all detectable showers which are in reach of the cameras, although the coverage of the southern hemisphere is much poorer than the northern section. We applied the same limiting factors for the detection as derived from the analysis of the outer regions of the major showers where these essentially are sources of small activity. The results are summarized in Table 3, the activity profiles are shown in Figure 9 and 10. Further, we comment on details of the showers in the text.

**145 ELY ($\eta$-Lyrids):** we find a clearly defined radiant despite the low activity over the period $\lambda_\odot = 46 - 53°$ which is almost exactly coinciding with the entry in the MDC list (see Table 3). The drift of the radiant as found from our data is shown in Figure 11. Our data show a smooth VR-profile (see Figure 9) with a maximum rate of VR = 2.1 at $\lambda_\odot = 50°$. Before 49° and after 52°, the rate is low with values of VR < 1. The agrees well with the activity profile of this shower which was recently included in the IMO's working list (Arlt & Rendtel, 2006).

**1 CAP ($\alpha$-Capricornids):** the radiant of this shower is quite close to the ecliptic and therefore interferes with radiants of the Antihelion Source. The major difference is the velocity which is close to 30 km/s for the Antihelion meteors and 24 km/s for the $\alpha$-Capricornids. The radiant is obvious in the interval between $\lambda_\odot = 109°$ and 138°. Although considered as a minor shower, the activity reaches a maximum VR = 5.2 at $\lambda_\odot = 125°$ and remains above 1.0 for all but the very last bin.

**12 KCG ($\kappa$-Cygnids):** this is another shower with a very low activity. We find VR ≥ 0.8 in the entire period $\lambda_\odot = 135° - 146°$ with a weak maximum of VR = 1.5 at $\lambda_\odot = 141°$ (profile in Figure 9). The radiant is well defined from 134° to 146° with increasing scatter towards the begin and end of the activity period (Figure 12). The entry in the MDC list gives values for the returns in 1993 and 2007 as well as an annual (average?) value. The radiant positions deviate significantly: the 1993 and 2007 radiants are by $5\overset{\circ}{.}3$ off in declination alone. Since our data sample includes data of 10 years, a sharp radiant position is not to be expected. Our analysis of short appearances (section 6.5) reveals another radiant at $\alpha = 288\overset{\circ}{.}2, \delta = +58\overset{\circ}{.}6$ in four bins (149°–152°). The declination fits well with the 2007 data, but the maximum VR is detected only at $\lambda_\odot = 152°$, while the 2007 maximum was observed 11° earlier. This shows that the $\kappa$-Cygnids behave more like a complex than like a single well defined shower.

**206 AUR (Aurigids):** this is the first shower of a series of further sources in the Auriga-Perseus region occurring from end-August to October. This established shower is known for its outbursts. The VR is not high because only the 2007 outburst was recorded by a few

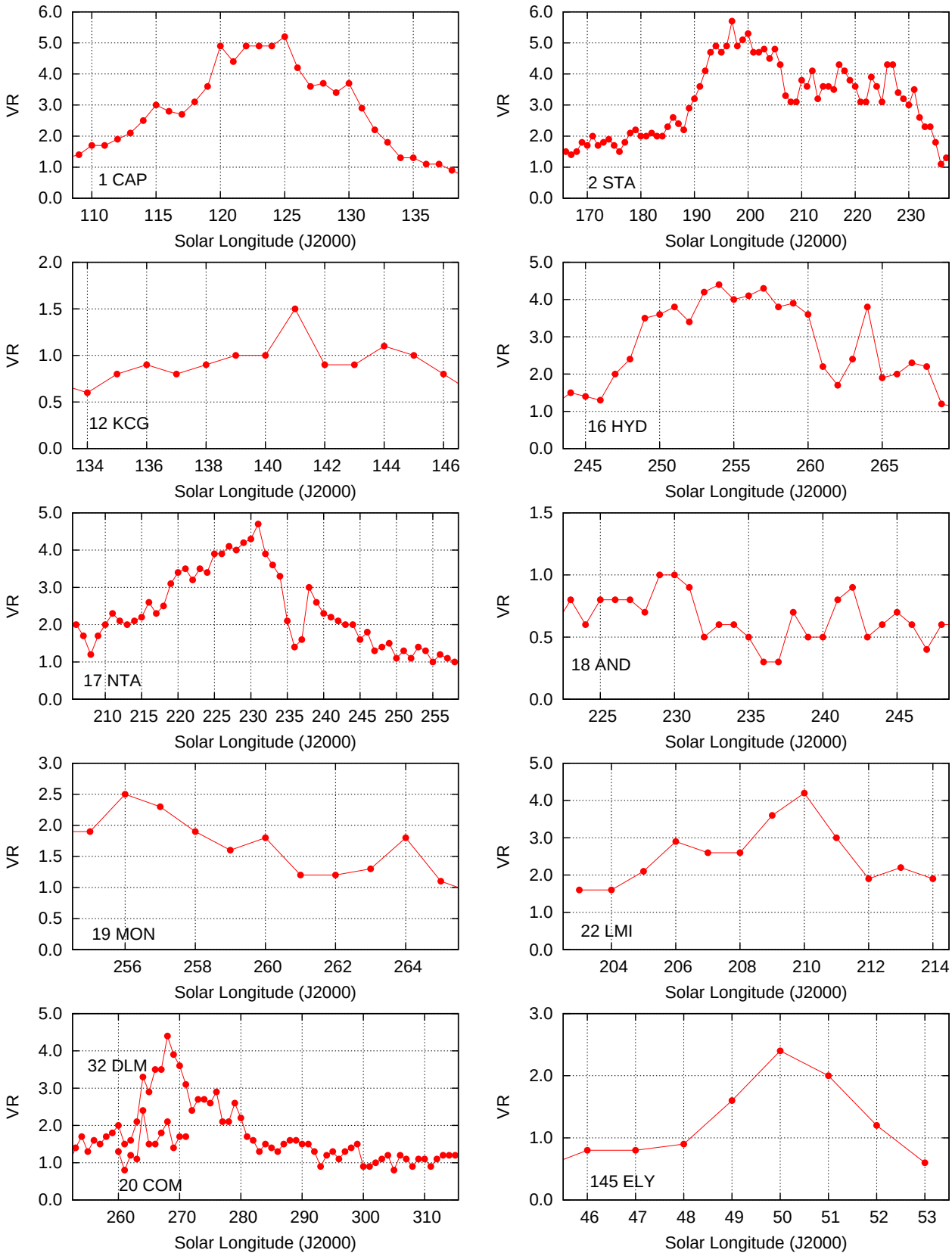


*Figure 9* – Activity profiles for the showers labelled as 'established' in the MDC list derived from our video data, sorted by the MDC shower numbers.

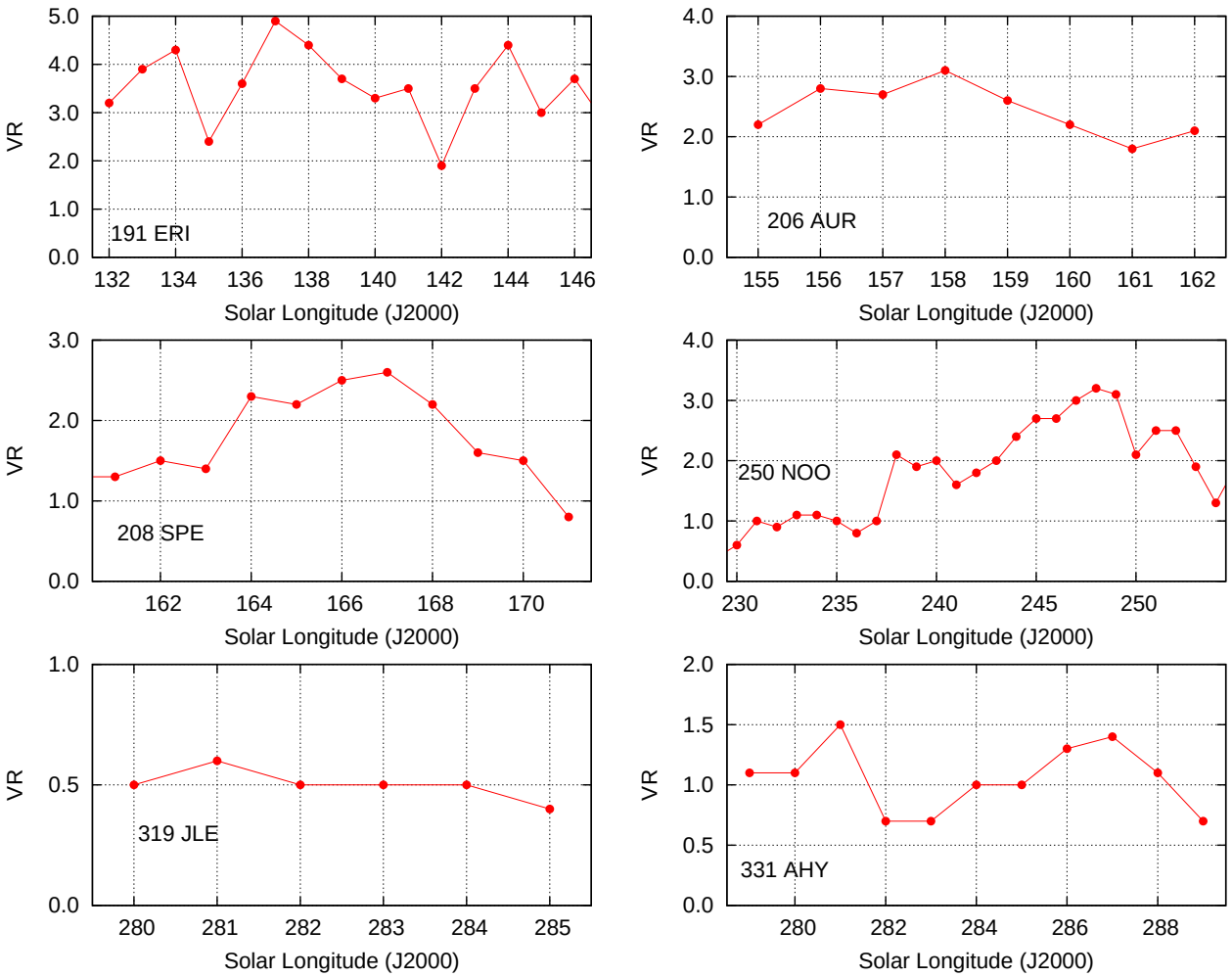


*Figure 10* – Activity profiles for the showers labelled as 'established' in the MDC list derived from our video data sorted by the MDC shower numbers.

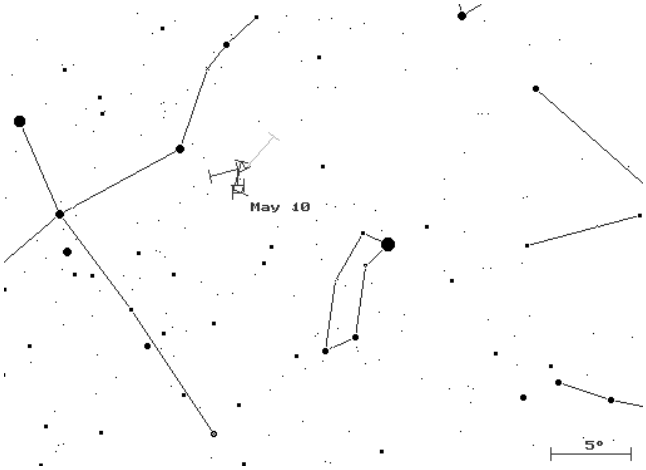


*Figure 11* – Radiant of the $\eta$-Lyrids derived from our video data.

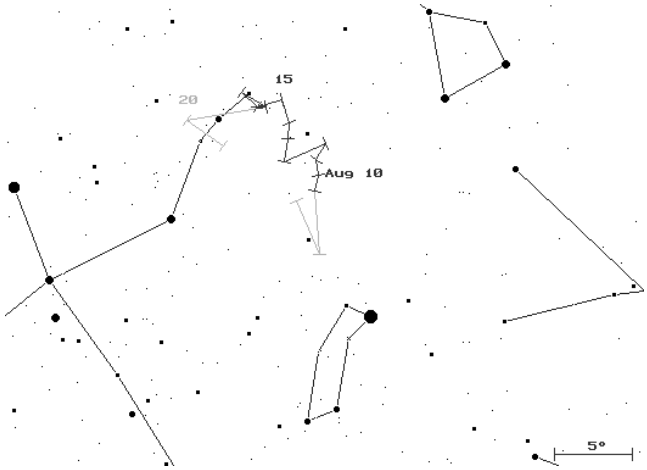


*Figure 12* – Radiant of the $\kappa$-Cygnids derived from our video data.

cameras of the Network. The last one before this happened in 1994.

**208 SPE (September $\varepsilon$-Perseids):** is the second shower of the series mentioned before. The VR reaches 2.6 and remains above 2.0 over five successive bins. It should be emphasized that the radiant obtained from the video data (48.°0, +39.°5) differs significantly from the position (60°, +47°) given in the IMO working list (Arlt & Rendtel, 2006). The position listed in the MDC files is 50.°2, +39.°4.

**191 ERI ($\eta$-Eridanids):** well detectable activity with a peak VR = 4.9 (Figure 10) and a consistent radiant drift fitting the position given in the list of established showers of the MDC.

**2 STA (Southern Taurids) / 17 NTA (Northern Taurids):** the two branches of the Taurids are

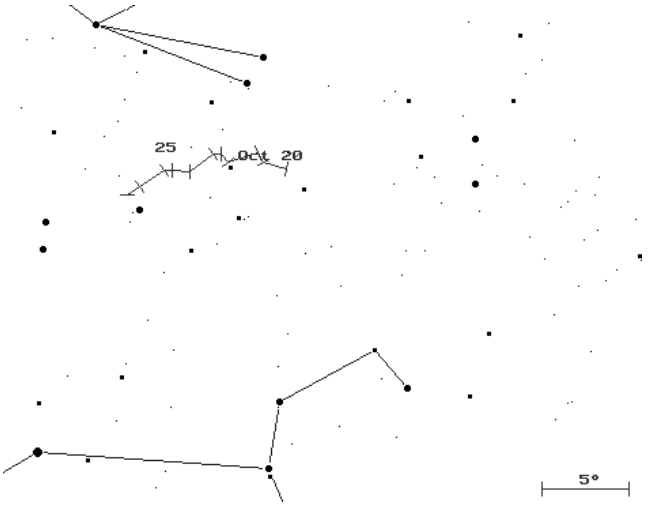


*Figure 13* – Radiant of the Leonis Minorids derived from the video data.

often assumed to coincide in their activity period with weak maxima separated by about two weeks. Our analysis as well as previous studies based on video and visual data show that the situation is somewhat different. The southern branch can be found much earlier, starting at $\lambda_\odot = 165°$ and lasting to 237°; the northern branch can be detected from 206° to 258°. The STA maximum at $\lambda_\odot = 197°$ reaches a VR = 5.7 and is higher than the value of 4.1 found for the NTA at $\lambda_\odot = 231°$. The maxima are thus separated by 34°in Solar longitude. The dip in VR near $\lambda_\odot = 236°$ is not real but an artefact due to the strong Leonid activity at that time.

**22 LMI (Leonis Minorids):** this is another shower which is active during the Orionid period. It produces rates which are clearly above the background. The radiant and activity is well defined from $\lambda_\odot = 203°$ to 214° (Figure 13) and the maximum VR = 4.2 occurs at $\lambda_\odot = 210°$.

**18 AND (Andromedids):** the annual Andromedid shower is a very weak source which can be traced over almost a month. There is no other source interfering with the shower meteor data because of their distinct very low velocity.

**250 NOO (November Orionids)**: only few shower compilations include this weak shower which we can trace from $\lambda_\odot = 233°$ to 254°. It shows a well defined radiant as well as an activity VR $\geq 1.5$ for most of the period (see Figure 10). The highest VR = 3.2 occurs at $\lambda_\odot = 248°$.

**16 HYD ($\sigma$-Hydrids):** this is a minor shower with a reasonably high activity over several bins. We find VR $\geq 4$ in five consecutive bins from 253° to 258° and a maximum VR = 4.7 at $\lambda_\odot = 254°$, also in good agreement with long-term visual results yielding an average maximum ZHR of about 3 (Rendtel & Arlt, 2009). The radiant is well defined from 244° to 269° with a slight deviation against the listed position of $\Delta\alpha = -4°$ and $\Delta\delta = +2°$ at the maximum date. The dip in VR near $\lambda_\odot = 262°$ is not real but an artefact due to the strong Geminid activity at that time.

**19 MON (December Monocerotids):** except the maximum date, all parameters coincide with the listed values. However, the activity is very low and has no pronounced maximum. Our highest VR = 2.5 occurs at 256° and thus 4° earlier than the catalogue date. The radiant can be traced until $\lambda_\odot = 268°$, but the rates are below our threshold in the bins at 266° and 267°.

**319 JLE (January Leonids):** the activity is just below the detection limit and if there were not the entry in the MDC list, we would not have not taken the detection as a signature of a shower. Since its rate remains below the threshold, we do not present an VR-profile here. However, the derived data of the radiant and velocity fit well with the tabulated values.

**331 AHY ($\alpha$-Hydrids):** another established shower with an activity very close to the detection limit. The shower was found automatically from 284° onwards, while the earlier activity was found when we checked for short duration showers. Probably the dominating Quadrantid activity caused that the minor source became undetectable. As in the case of the 319 JLE, the parameters fit well.

**Perseus-Auriga-showers in September and October:** we clearly detect showers in the Perseus-Auriga region from end-August to early October. These include the established shower 206 AUR (Aurigids) and 208 SPE (September $\varepsilon$-Perseids) which have been shortly discussed in the Section 6.2. Further examples are the $\beta$-Aurigids (210 BAU) and the October $\delta$-Aurigids (224 DAU), both having 'working status'. Especially the relation between the 208 SPE and 224 DAU has been analysed in previous papers (Rendtel 1993; Dubietis & Arlt, 2002). However, there is a larger number of showers detectable from this region which requires a more detailed analysis. Therefore we list only the two 'established' sources here.

**20 COM (Comae Berenicids) / 32 DLM (December Leonis Minorids):** this special case needs to be discussed in some detail. The Comae Berenicids (COM) have been in most shower compilations over many years. Recently, an analysis of video data (Molau, 2006) gave no hint at the existence of a radiant at the position listed in the IMO shower list as well as in the MDC list. The same analysis yielded a source which is obviously about 15° west of the radiant given for COM. Our present analysis shows that there are two sources (see the profiles shown in Figure 9). Weak activity from the 'old' radiant listed as Comae Berenicids (20 COM) can be detected in the period 260–271° (December 12–23), but definitively not longer. The other source which was clearly found already in the previous analysis is detectable over a much longer interval 253–315° (December 5 – February 4). The latter produces higher rates – we find a maximum VR = 4.6 at $\lambda_\odot = 268°$. This radiant perfectly fits the position given for the December Leonis Minorids (32 DLM) in the MDC list on December 14 ($\lambda_\odot = 262°$), although our analysis yields the maximum activity on December 20 ($\lambda_\odot = 268°$). The 20 COM is listed as an 'established shower' while the 32 DLM is in the working list.

The question is why this confusing situation occurred. Much of the past information is based on visual data and rather few photographs. Probably, most

of the activity was observed around the Geminid maximum (≈ 262°) and shortly thereafter, i.e. close to 268° (December 20) when both sources are detectable. Meteors occuring later are scarce and in most cases a reliable radiant determination is not possible. Another reason for uncertainties of the radiant position is the distribution of the observed meteors around the radiant. Meteors are observable mostly west and north of the radiant, which is the case especially before local midnight. Hence the position remains unreliable and two possible radiants cannot be distinguished because these are almost on one line. So it could easily be possible that both the existence of two radiants and the ceasing activity from the Comae Berenicids was not correctly observed. The conclusion from our analysis is clear: there are two showers. We find 20 COM for 260–271° (December 12–23) and the other, slightly stronger 32 DLM in the period 253–315° (December 5 – February 4).

## 6.3 MDC showers with working list status

The main achievement of the data set analysed here is the possibility to confirm the existence of showers with MDC working list status and to refine their parameters (radiant position and drift, velocity). Furthermore, we derive information about the video rate VR and thus of the activity period. This was not available for most of the showers compiled in the MDC working list. A summary of our results is listed in Table 4 and the VR-profiles are shown in the Figures 14 and 15. Details for selected cases are described in the text. It must be emphasized that these are all weak sources, often close to the detection limit. As described above, sections of the showers which remain below the thresholds set in the beginning have been omitted. Since the radiant data strongly depend on the number of associated meteors per bin, the drift values remain uncertain in some cases.

**136 SLE ($\sigma$-Leonids):** the radiant is found both in the standard analysis and the manual check for short period meteor activity. Although the VR is just at the detection threshold we listed it here, because the velocity of the meteors is very low and thus the source should be easily distinguishable from the background.

**190 BPE ($\beta$-Perseids):** the data seem to fit the entries in the MDC list quite well. However, the radiant drift is quite uncertain with jumps in consecutive bins. Either the sample is strongly affected by the Perseids with their radiant about 13°north, or the entire radiant is an artefact due to mis-aligned Perseids. Interestingly, the radiant is not found in SonotaCo's list based on orbit determinations.

**23 EGE ($\varepsilon$-Geminids):** this entry of the working list is quite similar to the established $\kappa$-Cygnid shower with low rates and no obvious maximum. The EGE rates are above 2 over the entire activity period. Slightly enhanced rates occur between $\lambda_\odot = 206°$ and 209° (Figure 14), coinciding with the Orionid maximum period. From Figure 16 it is obvious, that the radiant drift is well defined from 203° to 215°.

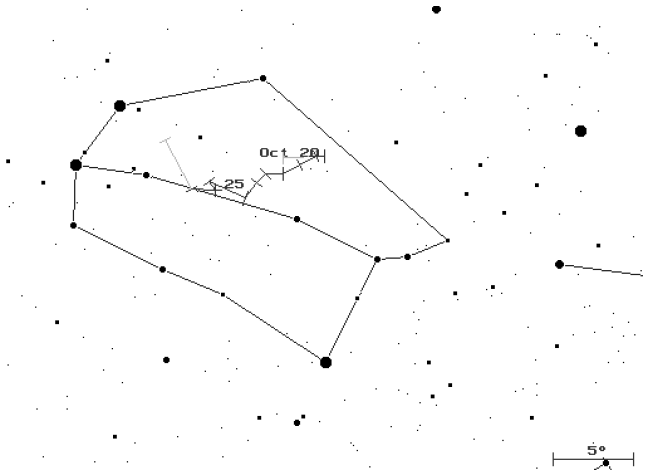


*Figure 16* – Radiant of the $\varepsilon$-Geminids derived from the video data.

**232 BCN (Daytime $\beta$-Cancrids):** interestingly, this shower can be seen in our video data. The right ascension and the velocity fit well with the data of the MDC list, but the declination is by 9° off, probably due to the fact that we can detect only very few meteors in the twilight period appearing to one side of the radiant.

## 6.4 New radiants found from the Network data

Many of the new radiants have been found in the months July and August. This is mainly due to the enormous amount of observational data. Over several years, the collection summarizes a substantial number also from weak sources.

**409 NCY, $\nu$-Cygnids:** this weak source produces a radiant about 30° east of the Lyrids. We carefully checked that these are not Lyrids which are sorted out from the major shower because they may have occurred far away from the radiant. Such meteors could produce a radiant further east with apparently slightly slower meteors. The substantial sample, the consistent radiant data found over the entire period and the large distance to the Lyrids radiant clearly indicate an independent source.

**410 DPI, $\delta$-Piscids:** the video rate VR exceeds 2.5 over the entire detection period, and the radiant drift is well defined. The radiant fits a (backwards) extrapolated drift of the July-Pegasids and the meteors have a similar velocity (67 km/s for JPE, 70 km/s here). However, the shower identified as July-Pegasids (see discussion in section 6.3) is significantly weaker than the source producing this activity. Therefore we propose this as a new radiant rather than the continuation of the July-Pegasids. It might be a similar case as we find it with the series of radiants in the Perseus-Auriga region in September-October.

**411 CAN, c-Andromedids:** the radiant (32°, +49°) is about 30° east of the (extrapolated) Perseid radiant on July 13. At this time, the activity of the Perseids is negligible, so that an interference with erroneously mis-identified and 'shifted' Perseids can be excluded. Of course, the similarity of the velocities (59 km/s) requires caution. The radiant drift shows

*Table 4* – Data of meteor showers included in the MDC working list, sorted by Solar longitude (J2000.0). The MDC list does not give an activity period for the showers of this list – so this is a new information derived from our analysis.

| Shower | Peak $\lambda_\odot$[°] | | Period $\lambda_\odot$[°] | Radiant position and drift [°] | | | | $V_\infty$ [km/s] | | Max. | Data |
|---|---|---|---|---|---|---|---|---|---|---|---|
| | (V) | (L) | (V) | $\alpha$ | $\Delta\alpha$ | $\delta$ | $\Delta\delta$ | (V) | (L) | VR | Met. |
| 40 ZCY $\zeta$-Cygnids | 16 | 20 | 7– 23 | 299.9 | +0.5 | +40.2 | +0.3 | 43.5 | 40.6 | 1.6 | 402 |
| 136 SLE $\sigma$-Leonids | 31 | 28 | 28– 35 | 202.9 | +1.2 | +4.7 | −0.2 | 20.0 | 25.5 | 0.7 | 269 |
| 343 HVI h-Virginids | 32 | 39 | 32– 35 | 214.1 | −1.3 | −11.4 | −1.6 | 24.1 | 21.8 | 1.6 | 192 |
| 175 JPE July Pegasids (*) | 108 | 107 | 105–126 | 347.2 | +0.9 | +11.1 | +0.2 | 68.1 | 62.3 | 1.6 | 591 |
| 184 GDR $\gamma$-Draconids | 125 | 125 | 120–127 | 280.9 | −0.2 | +50.7 | +0.2 | 27.3 | 28.5 | 1.6 | 428 |
| 190 BPE $\beta$-Perseids | 135 | 135 | 132–143 | 44.6 | +0.9 | +40.7 | −0.5 | 67.4 | 67.1 | 2.8 | 1176 |
| 197 AUD Aug. Draconids | 148 | 142 | 138–156 | 275.6 | +0.6 | +62.3 | +0.1 | 23.3 | 20.6 | 1.1 | 951 |
| 337 NUE $\nu$-Eridanids | 164 | 168 | 161–181 | 66.7 | +0.6 | −0.5 | +0.5 | 67.7 | 66.8 | 5.1 | 1185 |
| 234 EPC Oct. $\varepsilon$-Piscids | 196 | 195 | 194–198 | 1.2 | +0.3 | +14.0 | +0.9 | 19.2 | 24.4 | 0.8 | 210 |
| 226 ZTA $\zeta$-Taurids | 203 | 196 | 199–204 | 79.7 | +0.8 | +12.2 | −0.8 | 60.6 | 68.1 | 0.8 | 294 |
| 333 OCU Oct. Ursae Majorids | 202 | 202 | 199–206 | 143.8 | +1.9 | +63.3 | −0.2 | 53.0 | 55.2 | 2.5 | 533 |
| 237 SSA $\sigma$-Arietids | 206 | 202 | 200–210 | 50.7 | +1.1 | +22.1 | 0.0 | 45.5 | 42.0 | 1.0 | 475 |
| 23 EGE $\varepsilon$-Geminids | 206 | 206 | 203–214 | 101.8 | +0.9 | +28.2 | −0.2 | 70.4 | 68.8 | 2.8 | 1134 |
| 241 OUI Oct. Ursae Minorids | 211 | 208 | 206–214 | 273.4 | −1.1 | +74.3 | −0.3 | 27.5 | 32.9 | 0.8 | 308 |
| 232 BCN Dayt. $\beta$-Cancrids | 214 | 213 | 212–221 | 110.5 | +0.8 | −6.1 | +1.2 | 65.1 | 67.0 | 3.4 | 386 |
| 333 OER $o$-Eridanids | 232 | 235 | 231–238 | 60.2 | +0.2 | −1.3 | −0.2 | 27.1 | 29.1 | 1.2 | 229 |
| 339 PSU $\psi$-Ursae Majorids | 253 | 253 | 247–261 | 168.3 | +1.5 | +43.1 | −0.3 | 61.1 | 61.7 | 1.8 | 432 |
| 336 KDR Dec. $\kappa$-Draconids | 251 | 250 | 248–254 | 185.4 | +0.6 | +71.5 | −1.2 | 42.9 | 44.8 | 2.5 | 225 |
| 334 DAD Dec. $\alpha$-Draconids | 253 | 257 | 252–264 | 203.6 | +0.8 | +60.1 | −0.3 | 43.8 | 43.1 | 1.7 | 531 |

(*) JPE: velocity drift observed −0.16 km/s per 1° in Solar longitude

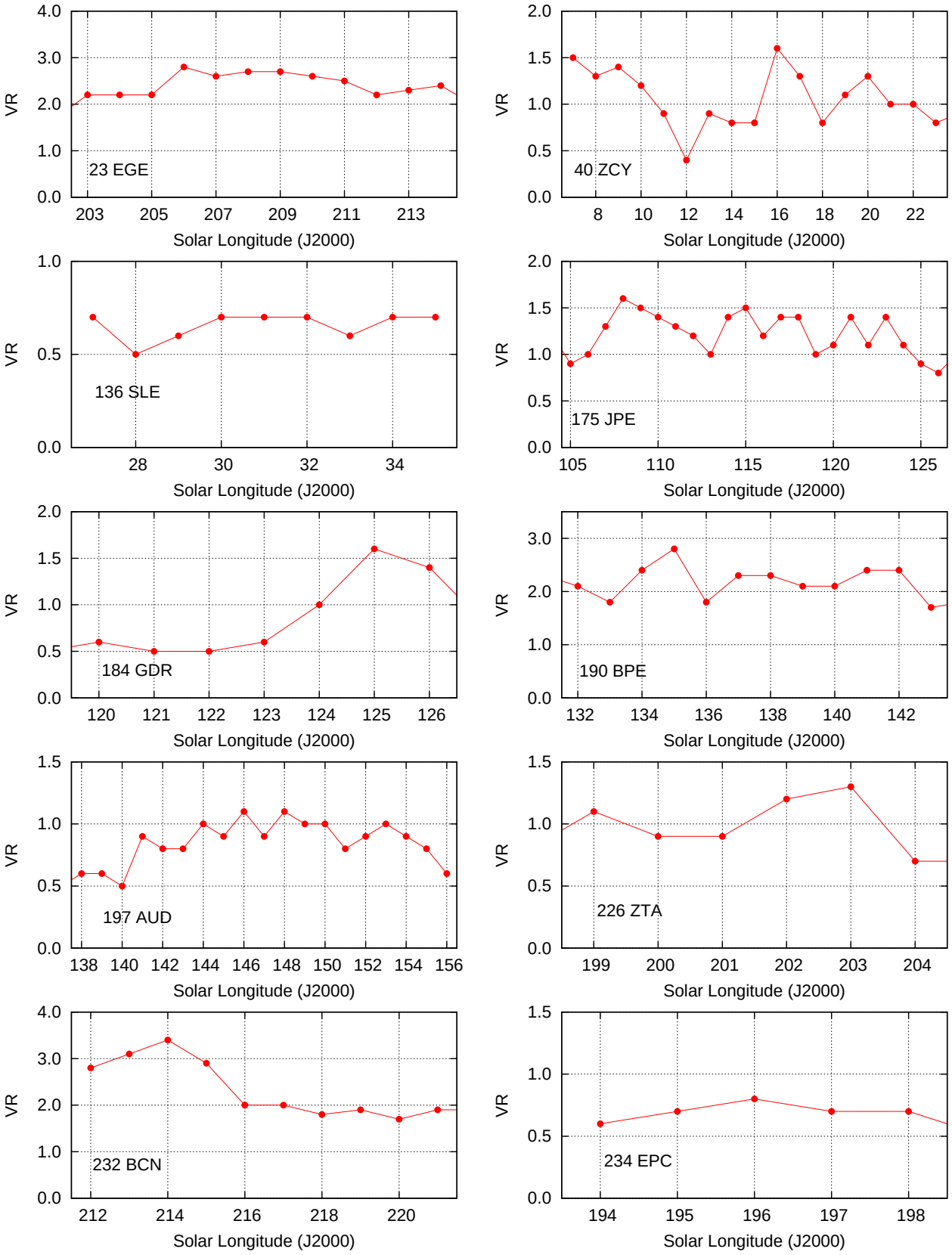


*Figure 14* – Activity profiles for the showers of the 'working list' derived from our video data, sorted by the MDC shower numbers.

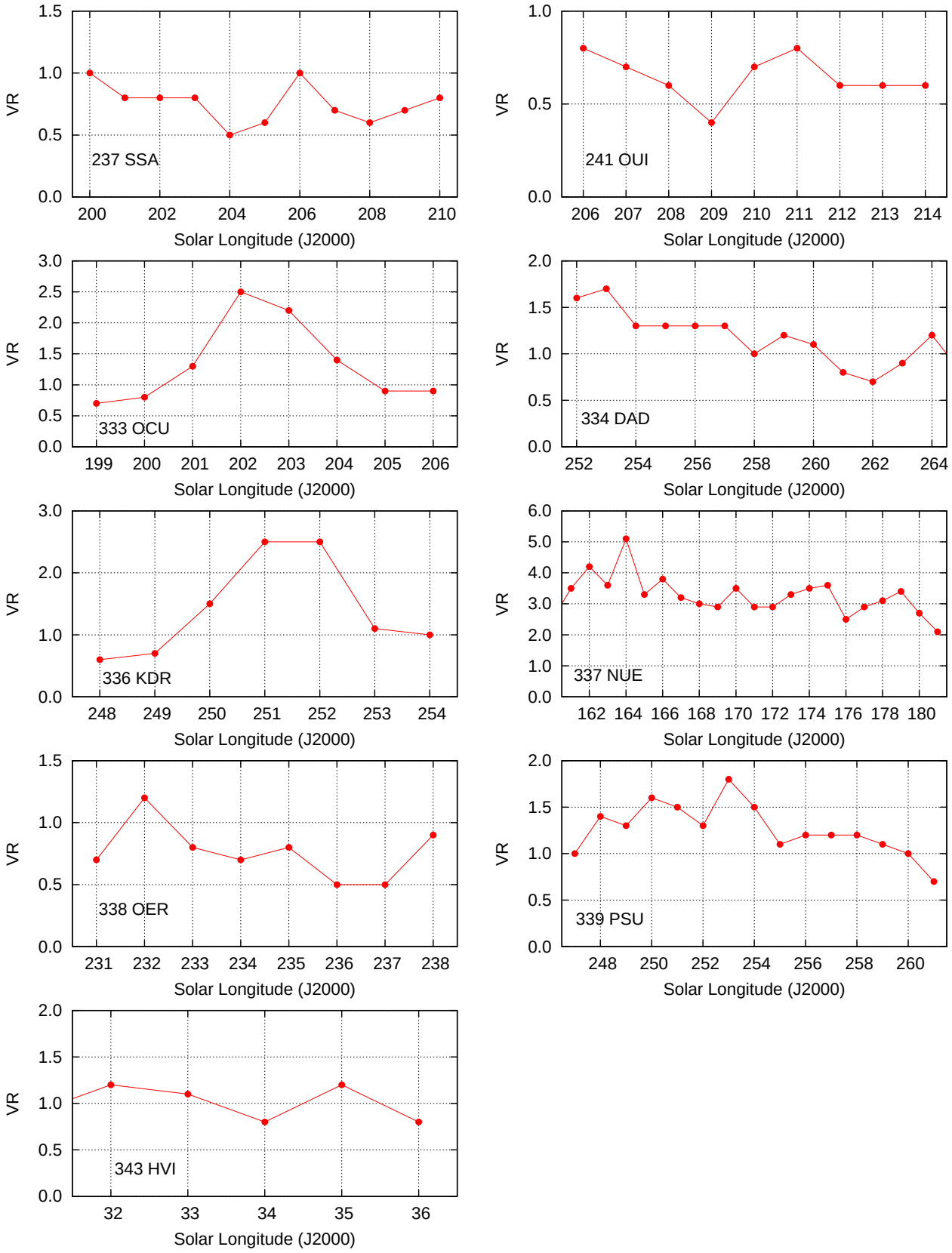


*Figure 15* – Activity profiles for the showers of the 'working list' derived from our video data, sorted by the MDC shower numbers.

*Table 5* – Data of meteor showers found in the IMO Video Meteor Network data, sorted by Solar longitude (J2000.0). The activity data expressed in terms of the video rate (VR) described above is summarized in Figure 17.

| Shower | Max. ($\lambda_\odot$) [°] | Period ($\lambda_\odot$) [°] | Radiant position and drift [°] $\alpha$ | $\Delta\alpha$ | $\delta$ | $\Delta\delta$ | $V_\infty$ [km/s] | VR | Data Met. |
|---|---|---|---|---|---|---|---|---|---|
| 409 NCY $\nu$-Cygnids | 30 | 28– 44 | 305.2 | +1.8 | +39.4 | +0.7 | 42 | 1.8 | 508 |
| 410 DPI $\delta$-Piscids | 92 | 89– 93 | 10.9 | +0.3 | +5.5 | +0.4 | 71 | 4.2 | 105 |
| 411 CAN c-Andromedids | 110 | 102–114 | 32.4 | +1.0 | +48.4 | +0.4 | 59 | 2.3 | 491 |
| 412 FOP f-Ophiuchids | 98 | 96–100 | 266.4 | +4.0 | +8.5 | −0.6 | 21 | 0.7 | 81 |
| 413 MUL $\mu$-Lyrids | 116 | 113–118 | 273.1 | −0.0 | +39.4 | −0.5 | 23 | 0.6 | 129 |
| 414 ATR $\alpha$-Triangulids | 120 | 119–124 | 28.9 | −0.2 | +28.1 | −2.2 | 71 | 3.6 | 192 |
| 73 ZDR $\zeta$-Draconids | 122 | 122–126 | 261.7 | +5.8 | +67.8 | +0.8 | 25 | 0.6 | 148 |
| 415 AUP August Piscids | 132 | 130–137 | 7.5 | +0.9 | +18.3 | +0.1 | 66 | 1.1 | 433 |
| 81 SLY September Lyncids | 167 | 165–172 | 107.4 | +1.7 | +55.0 | +0.3 | 61 | 1.4 | 467 |
| 416 SIC Sep. $\iota$-Cassiopeiids | 169 | 166–171 | 36.7 | −0.2 | +65.0 | +1.0 | 50 | 0.8 | 278 |
| 417 ETT $\eta$-Taurids | 211 | 211–221 | 55.5 | +0.9 | +23.7 | −0.0 | 47 | 1.2 | 323 |
| 418 BHE $\beta$-Herculids | 324 | 322–326 | 246.0 | +0.9 | +23.5 | −0.9 | 55.5 | 1.4 | 99 |

some 'irregular' jumps near $\lambda_\odot = 100 - 102°$ while it is smooth after this date until 114°. The VR varies around 2 with a maximum at $\lambda_\odot = 110°$, i.e. July 13, which coincides approximately with the onset of the 'regular' Perseids. We give 103–114° as the activity period because of the inconsistent early position mentioned above; if this were not the case, we could trace the radiant back to $\lambda_\odot = 96°$.

**412 FOP, f-Ophiuchids:** this source is very weak and thus close to the detection limit. The low velocity of the shower meteors at 21 km/s should remarkably decrease the effect of accidentially aligned sporadic meteors. Particularly at the end of the detection period, after $\lambda_\odot = 104°$, the scatter of the radiant position becomes larger than the limits set for our study. Hence we give an activity period $\lambda_\odot = 99 - 104°$.

**413 MUL, $\mu$-Lyrids:** the radiant at 273°, +39°, could also be named $\vartheta$ Her. This very weak source is another case with a peculiar low $V_\infty = 23$ km/s. As in the case of the f-Ophiuchids, there are no other sources in a wider surrounding region of the sky. The radiant drift is not well defined, but the position is at about 62° ecliptical latitude.

**414 ATR, $\alpha$-Triangulids:** like in September with the Perseus-Auriga showers, there may be more than one source in the vicinity of the (north) apex region in July. The July-Pegasids have been described in the previous section. Meteors from this radiant in Triangulum are found at 71 km/s. An effect from other known sources is not expected because the other radiants are far enough from the radiant.

**73 ZDR, $\zeta$-Draconids:** this radiant is another case formed by slow meteors at 25 km/s coming from almost 70° ecliptical latitude. Like the other two sources with similar low velocity meteors, the video rate VR remains close to the detection limit over the entire period. The drift is not well defined towards the end of the given period. A shower designated as ZDR was already listed in the MDC list. The stored data of radiant position and velocity are based on Lindblad (1971). In this work, two orbits were identified. Similar (slow) meteors give further radiants in Hercules and Cygnus. Jenniskens (2006, p. 712) lists two, the 88 ODR and 182 OCY at 116 and 117°, respectively. The low velocity is common to all these entries. The shower identified from our video data is new and indeed near $\zeta$ Draconis. Hence it was decided in the Task Group on Meteor Shower Nomenclature (Jenniskens et al., 2009), to keep the existing code and to use the new data obtained from this analysis.

**415 AUP, August Piscids:** this source might have some similarity to the $\alpha$-Triangulids discussed before. The radiant is about 15° north of the ecliptic and the velocity of the meteors is rather high (66 km/s). We can trace the radiant for some more days than listed here, but the uncertainties of the position become quite large after $\lambda_\odot = 138°$.

**81 SLY, September Lyncids:** this shower may be associated with others radiating from the Perseus-Auriga region in autumn with similar velocities, such as AUR, SPE or DAU. This radiant is the northernmost found in the region. The radiant can be consistently traced over the entire period from 165° to 172°. Two earlier bins at 162 and 163° also show the radiant with similar strength, but with an uncertain radiant drift. The entry of the 81 SLY also goes back to Lindblad's (1971) paper and the shower data is based on very few graphically reduced photographic orbits. Like in the case of the 73 ZDR, the Task Group proposed to keep the code for the shower but to replace the data with those obtained from our video meteor analysis. Further details are discussed in Section 6.4.

**416 SIC, September $\iota$-Cassiopeids:** we find this shower at $\alpha = 34°, \delta = +65$, with $V_\infty = 50$ km/s in a rather short period around $\lambda_\odot = 169°$. Interferences from other known sources can be excluded.

**417 ETT, $\eta$-Taurids:** in the interval $\lambda_\odot = 211 - 221°$ (Max. 211°), we detect the radiant at $\alpha = 54°, \delta = +24°$; $V_\infty = 47$ km/s, near $\eta$ Tau. Actually, the analysis yields two detections, which obviously define one radiant near the Pleiades with a reliable video rate and a well defined radiant.

**418 BHE, $\beta$-Herculids:** is a shower found from the short activity period check (see Section 6.5). It can be found between $\lambda_\odot = 322$ and 326°. This is a period with a generally low meteor activity and thus suited for the detection of weak sources. The VR of 1.4 is well above the threshold value.

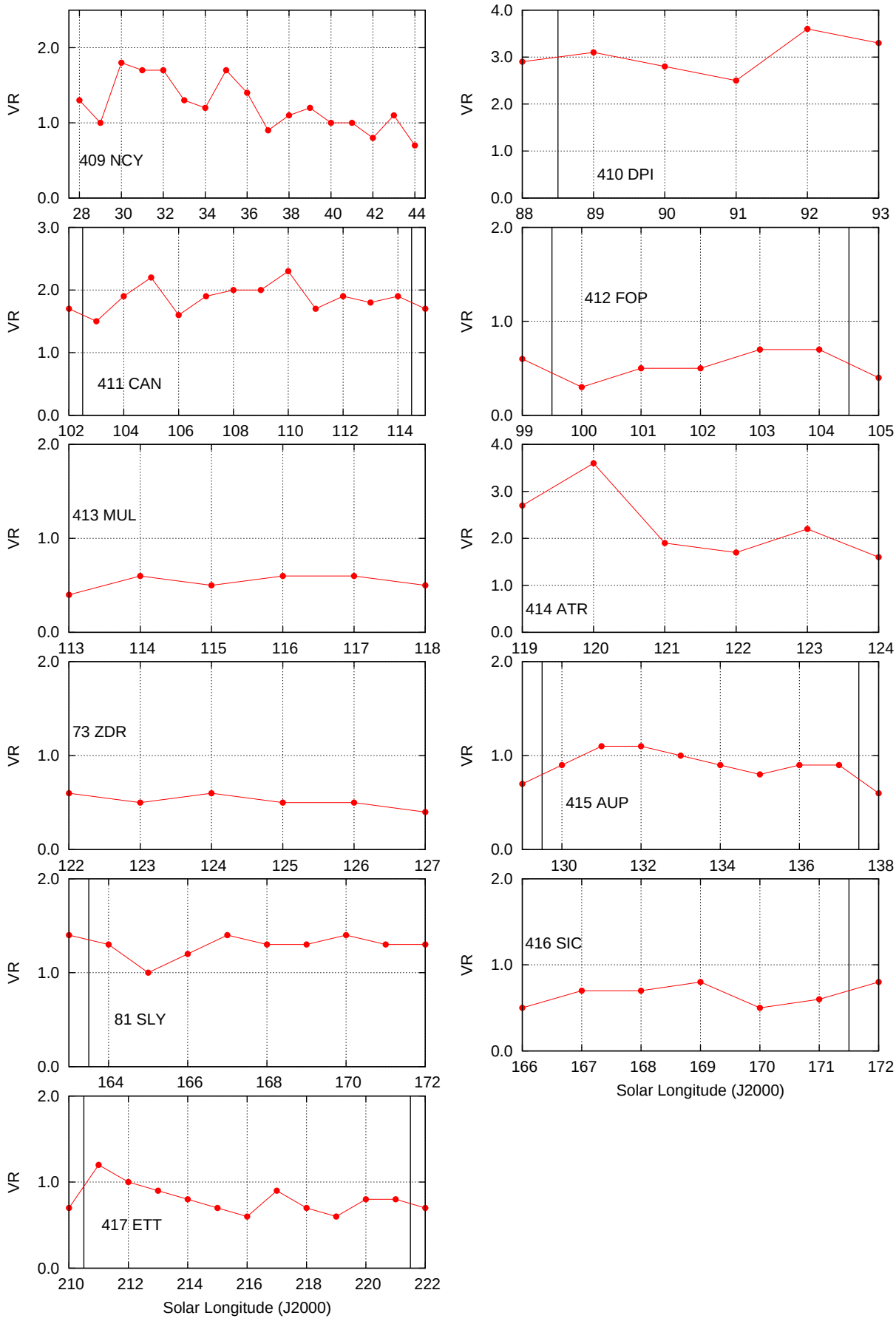


*Figure 17* – Activity profiles of the new showers found from the video data. The vertical lines indicate the limits of the activity period defined by the VR *and* the radiant position. The graphs are sorted as in Table 5.

*Table 6* – Showers of short duration which were detected only in 3–4° intervals of Solar longitude according to the described manual refinement. (V) refers to the results from our video data, (L) to the MDC list.

| Shower | Peak and period $\lambda_\odot$[°] | | | Rad. position, drift (V) [°] | | | | Radiant (L) | | $V_\infty$ [km/s] | | Max. | Data |
|---|---|---|---|---|---|---|---|---|---|---|---|---|---|
| | (V) | (L) | (V) | $\alpha$ | $\Delta\alpha$ | $\delta$ | $\Delta\delta$ | $\alpha$ | $\delta$ | (V) | (L) | VR | Met. |
| 43 ZSE $\zeta$-Serpentids | 4 | 365 | 3– 7 | 256.2 | +2.1 | −4.1 | +0.4 | 266.3 | −6.3 | 63.8 | 68.4 | 1.5 | 86 |
| 136 SLE $\sigma$-Leonids | 23 | 28 | 21– 24 | 199.5 | −0.5 | +3.6 | −0.6 | 192.6 | +3.1 | 22.7 | 25.6 | 1.1 | 129 |
| 149 NOP N. May Ophiuchids | 52 | 50 | 47– 53 | 237.1 | +1.6 | −8.2 | +0.9 | 249.0 | −14.0 | 28.0 | 30.0 | 1.8 | 291 |
| 337 NUE $\nu$-Eridanids | 165 | 168 | 162–165 | 74.7 | +0.6 | +0.3 | −1.9 | 68.7 | +1.1 | 67.0 | 66.8 | 3.7 | 157 |
| 81 SLY Sept. Lyncids | 186 | 185 | 186–189 | 110.2 | −2.9 | +48.4 | −0.7 | 110.0 | +47.9 | 67.7 | 66 | 1.6 | 237 |
| 323 XCB $\xi$-Coronae Borealids | 295 | 295 | 290–295 | 248.3 | −0.2 | +29.2 | −0.1 | 244.8 | +31.1 | 50.1 | 45.7 | 1.2 | 105 |
| 97 SCC South. $\delta$-Cancrids | 298 | 296 | 294–298 | 131.5 | +1.7 | +10.6 | −1.0 | 134.1 | +10.1 | 28.7 | 27.6 | 0.9 | 134 |
| 101 PIH $\pi$-Hydrids | 319 | 317 | 315–319 | 215.2 | +1.0 | −26.2 | −1.9 | 210.3 | −23.0 | 69.7 | 71.6 | 3.2 | 88 |

## 6.5 Short duration showers

The standard procedure as decribed above requires a radiant to be detected over five degrees in Solar longitude. Consequently, it omits short duration showers, such as the Draconids. In order to find active sources which are detectable over a shorter period of time, we run an additional analysis allowing for a minimum of three degrees length only. Of course, many known sources re-appeared and several unreliable sources showed up, which is why we concentrated only on strong sources or those fitting to showers from the MDC list. Overall, nine additional sources have been detected, among these one new source, named 418 BHE ($\beta$-Herculids; see Section 6.4). The results from the short interval analysis are summarized in Table 6.

The procedure finds radiants which fit the data of the Northern May Ophiuchids (149 NOP) reasonably well in two separate intervals. Both radiants differ from the listed position, and the velocity fits better in the second period ($\lambda_\odot = 47° - 53°$) which is included in Table 6.

81 SLY is found not only in the short interval listed in Table 6 but was detected automatically by the standard procedure. This procedure reveals the SLY in two periods (179°–184° and 189°-194°) with an interruption in the center. The radiant is close to the apex, which is also detected as a relatively strong source in this interval. Hence we expect an interference from apex meteors leading to an uncertain radiant position of the weak September Lyncids. Consequently, we list the shower only in the central short interval in which the fit with the listed data is best and VR = 1.6. A recent discussion in the Task Group (Jenniskens, 2009) as well as the analysis of our data set yielded a likely connection between the 81 SLY as they were included in the existing MDC list on the one hand and our new detection (now the 81 SLY as described in the Section 6.4 and Table 5) and the short-duration activity discussed here on the other hand. However, the fact that our analysis yielded two detections (the 'new' radiant and the slightly deviating short duration shower) indicates, that the case is not yet completely solved. At the moment, we cannot match all detections to describe one continuous source. We either see one source at different activity intervals or more than one shower (with similar physical data) being part of the already mentioned complex in the Perseus-Auriga region. Details will be presented in the respective upcoming analysis.

## 6.6 Established showers from the MDC list not found in our data

Many, but not all showers that are marked as established in the MDC list were found in our analysis. There are several reasons why a shower may have been missed.

(i) The shower is too weak or occurs at a time of year that is poorly covered by observations. Chances for this are low, because our total sample has a good coverage of the entire year.

(ii) The activity interval of the shower is too short, or the shower is not permanently active: We will have missed showers, which show only once in a few years significant activity or who are active for only one or two days. AMO and JBO are such showers.

(iii) The radiant lies far south. Most meteor observations were obtained from the northern hemisphere. There is also a subset of about 15 000 meteors recorded from Australia, but in general the coverage of the southern hemisphere is poor. The geographical distribution of the cameras should allow to detect all significant meteor showers north of $\delta \approx -25°$. 'Established' showers south of this limit are ACE, BHY, GNO, PHO, PUP, and PPU.

(iv) The meteors are too faint to be detected by video. If meteor showers were detected by radar, they might be composed of meteors beyond the limit of video observation.

(v) The meteors occur at daytime. Most daytime meteor showers cannot be detected in the optical domain.

Several established MDC list showers were missing in our analysis. So we checked the original radiant set of the analysis per Solar longitude bin whether we find traces of these showers.

**102 ACE ($\alpha$-Centaurids):** no traces of this far southern radiant, but our sample includes only few respective data.

**11 EVI ($\eta$-Virginids):** radiant is clearly visible in our data. As it is close to the antihelion source, we have not listed this shower separately here. Another shower, 123 NVI (Northern March Viginids), has essentially the same position but a lower velocity. Our data fits the 11 EVI.

**27 KSE ($\kappa$-Serpentids):** in the interval 14–16° we find weak radiants which could fit the KSE data. $\lambda_\odot$=14°: 230.°5, +12.°5, 43 km/s; $\lambda_\odot$=15°: 227.°4, +12.°5, 45 km/s; $\lambda_\odot$=16°: 221.°8, +17.°5, 47 km/s.

**21 AVB ($\alpha$-Virginids):** in our analysis we find one weak detection in the region which does not fit well. It is located at 197°, −6.°5, $V_\infty$=20 km/s at 29° Solar longitude.

**137 PPU ($\pi$-Puppids):** not found in our analysis due to its southern position and the low activity except its outbursts.

**55 ASC ($\alpha$-Scorpiids:)** this is another radiant which is near the Antihelion source. Our analysis yields two detections at 54° and 55° which are more than 10° northeast at 256°, −23.°5 and correspond to $V_\infty$ = 37 km/s.

**61 TAH ($\tau$-Herculids):** no signs in our analysis.

**165 SZC (Southern June Aquilids):** could be a very short duration shower. At $\lambda_\odot = 79°$ find a radiant at 302.°8, −33.°5, $V_\infty$ = 35.0 km/s which fits the listed values reasonably. The next two bins also show a radiant close to the position (304°, −34°) but composed of meteors with 45 km/s.

**164 NZC (Northern June Aquilids):** can be detected in our results, although the routine matched our data with the 179 SCA ($\sigma$-Capriconids). Both are not too far from the Antihelion source.

**63 COR (Corvids):** $V_\infty = 14.4$ km/s – meteors at such very low velocities should be easily distinguished from the background, but the analysis yields no sign of this shower. During the observed years there was obviously no activity present.

**170 JBO (June Bootids):** is found only as an extremely weak detection at $\lambda_\odot = 97°$ ($229\overset{\circ}{.}5, +43\overset{\circ}{.}5$, $V_\infty = 18.0$ km/s). As found in other analyses, the activity is essentially zero outside the outburst intervals.

**187 PCA ($\psi$-Cassiopeiids):** despite the position far from other sources and not interfering with activity periods of other showers, nothing is found in our data.

**183 PAU (Piscis Austrinids):** we find weak signs earlier between 113 and 117°, but the data remained below our thresholds for shower detection.

**3 SIA (Southern $\iota$-Aquariids):** is difficult to separate from the strong 5 SDA. The analysis gives radiants in the vicinity of the SDA over the activity period, espcially at 127° and 130°, but no consistent radiant which could be identified as SIA.

**198 BHY ($\beta$-Hydrusids):** lacks from the small amount of data for this far southern radiant.

**233 OCC (October Capricornids):** nothing is found in our data.

**281 OCT (October Camelopardalids):** radiant $\alpha = 168\overset{\circ}{.}3, \delta = +78\overset{\circ}{.}0, V_\infty = 44.5$ km/s at $\lambda_\odot = 192.9°$ is clearly visible between 192 and 193°, but not found by the automatic procedure because of the very short activity interval. The maximum video rate is VR = 2.0 and thus above the thresholds (based on 118 meteors).

**9 DRA (October Draconids):** the radiant $\alpha = 262°, +56°, V_\infty = 19$ km/s at $\lambda_\odot = 195\overset{\circ}{.}5$ is detected between 195 and 196°, but the duration is too short for the automatic procedure. The maximum video rate is VR = 0.8 (only 80 meteors as the sample does not include any period of enhanced activity).

**246 AMO ($\alpha$-Monocerotids):** this is an established shower which cannot be found in our analysis. It is famous for its short-lived outbursts of which the last was observed in 1995. In all other years, the rates remained close to the detection limit. Our data show signs of a very weak AMO activity. However, the radiant deviates from the outburst position in right ascension and declination. Actually, the analysing procedure yields two radiants on both sides of the known position with the more northern one producing a higher rate (maximum VR = 2.7 at 238°). Furthermore, we find the best fitting velocity deviates by −3 km/s for the radiant south of the listed position, but +4 km/s for the radiant north of the listed position. This indicates some artefacts, possibly due to uneven distribution of associated shower meteors around the radiant position.

**254 PHO (Phoenicids):** lacks from the small amount of data for this southern radiant.

**256 ORN (Northern $\chi$-Orionids:** is part of the Antihelion source and continues the Southern Taurid activity. The analysis detects the radiant, but we do not analyse it here separately.

Not unexpectedly, the daytime (D.) showers 141 DCP (D. $\chi$-Piscids), 144 APS (D. April Piscids), 153 OCE (Southern D. $\omega$-Cetids), 171 ARI (D. Arietids), 172 ZPE (D. $\zeta$-Perseids), 173 BTA (D. $\beta$-Taurids), 188 XRI (D. $\xi$-Orionids) and 221 DSX (D. Sexantids) did not occur in our analysis.

## 7 Summary and Conclusions

As summary, we show two figures that present all meteor shower radiants detected in the IMO Video Meteor Database in a sinusoidal projection with right ascension on the abscissa and declination on the ordinate (Figure 18). The meteor shower velocity is color coded. It is worth to compare the plot with the presentation of the Japanese results in SonotaCo (2009), Figure 5 and back cover of the respective WGN issue. All significant features are found in both plots. Note, however, that the plots are created in slightly different ways. From double-station data like the SonotaCo analysis, a unique radiant point (right acsencion, declination, velocity) is obtained for each individual meteor recorded by two or more stations. Hence, each dot represents a single meteor in their graph. From single station data as presented here, the radiant position is ambiguous: For each meteor, there are several possible radiant points with different positions and velocities along the backward trace. Only when large data sets are analysed in a statistical way, we find radiant points composed by several meteors. These radiant points are depicted in Figure 18, i.e. here each dot represents approximately 50 single station meteors on average, with a range between 10 and 10 000. Meteor showers show up as cluster of points in the SonotaCo plot, but they would get lost in our graph because even thousands of meteors are represented by a single dot. For this reason, we coded the meteor number with the brightness: the brighter a dot, the more meteors contributed to the radiant.

Figure 19 is our version of the corresponding Figure 6 in the SonotaCo paper. Here, the abscissa represents the difference between the ecliptical radiant longitude and the solar longitude, and the ordinate the ecliptical latitude of the radiant. The similarity of both plots is amazing and underlines the abilities of the method presented here.

Recent radiant searches (SonotaCo, 2009; Brown et al., 2008, 2009) gave not only new positions of shower radiants but increased also our knowledge about the physical parameters and the extensions of the streams. The list of nine major and 44 minor showers analysed here show that the procedures work well. Cross-comparisons also demonstrate that the results obtained from independent data sets and applying different methods reveal consistent and therefore reliable results. Hence the detection of twelve new showers is not surprising. Further, the shift in velocity over the activity period found here and confirmed for several examples from SonotaCo's independent data sample demonstrates that the continuous collection of data is not only useful for an increasing accuracy of existing data but also for new results.

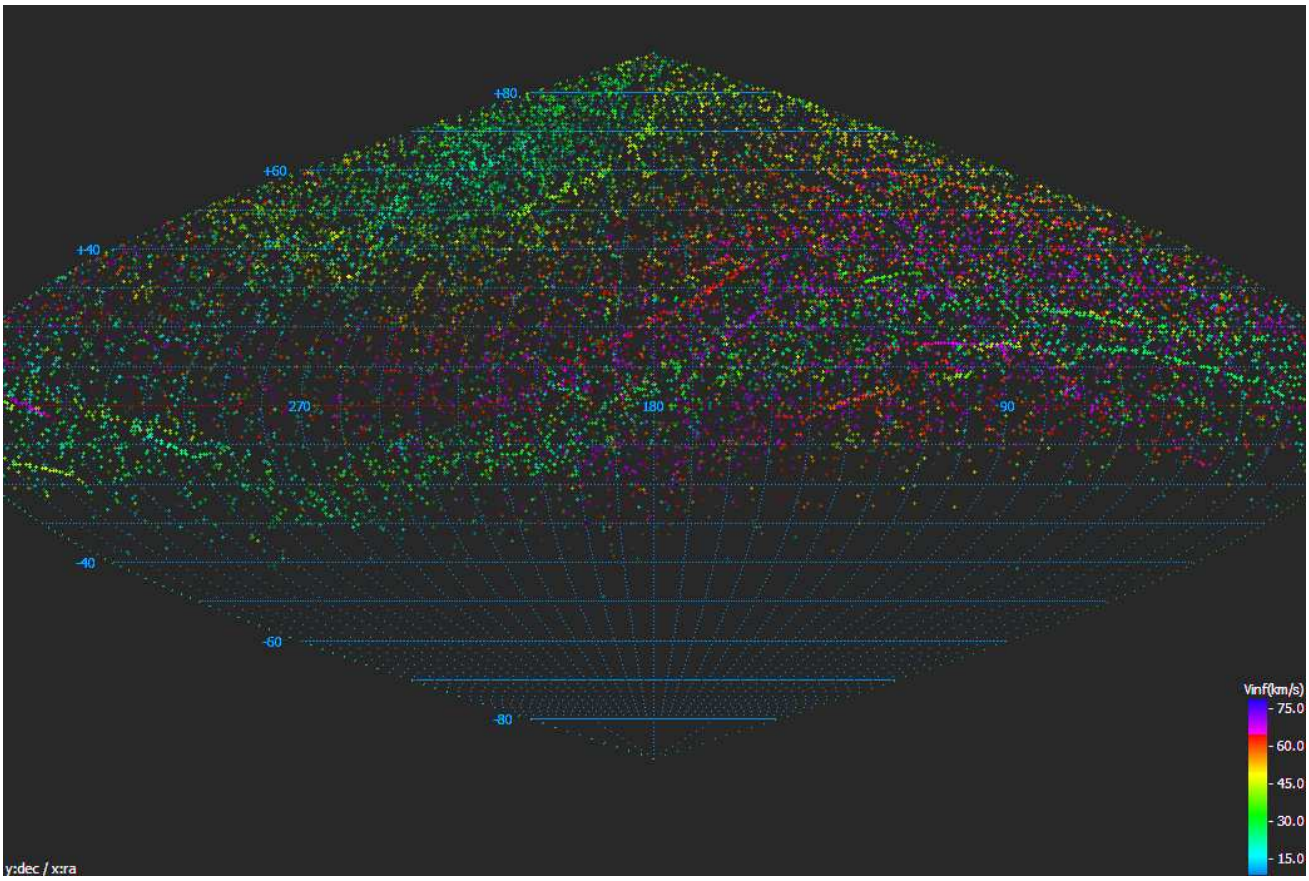


*Figure 18* – Distribution of radiants detected in the IMO Video Meteor Database over right ascension and declination in a sinusoidal projection. The brightness of each spot represents the number of meteors that contributed to the radiant, and the meteor shower velocity is coded in the color (reproduced on the back cover).

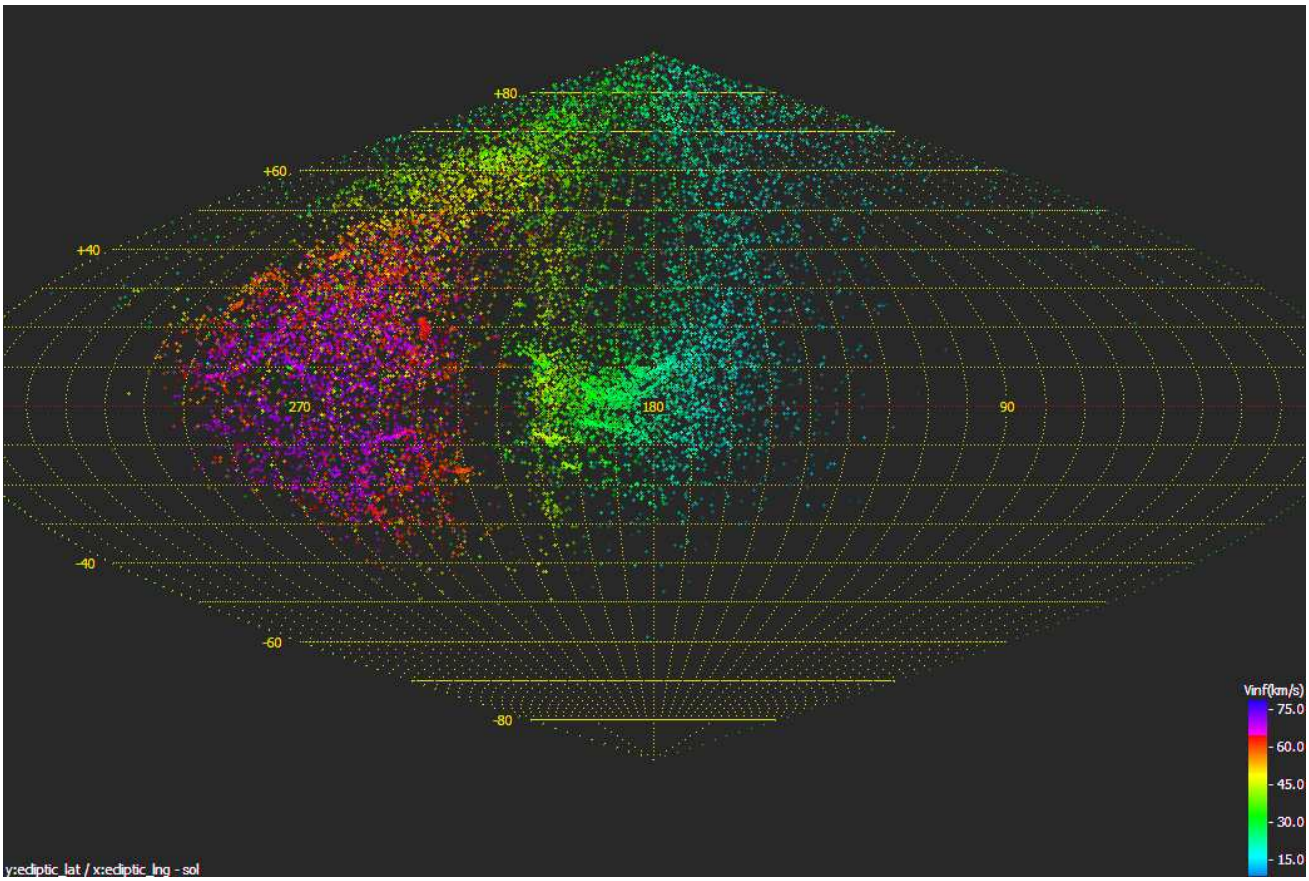


*Figure 19* – Distribution of radiants detected in the IMO Video Meteor Database in Sun-centered ecliptical coordinates with the ecliptical radiant longitude minus the solar longitude as x-axis, and the ecliptical latitude as y-axis.

## 8 Acknowledgements:

We are in debt of all video camera operators (see Table 1) who provide us with their meteor data on a regular basis and lay the foundation for analyses like this. Even if the observation is largely automated these days, it still requires a lot of passion and patience to set up a video system, get used to the analysis software, operate one or even multiple cameras for several years and process the data before they are collected in the central database.

In particular, we like to thank the Japanese meteor observer, UFO* programmer and meteor network operator SonotaCo. In recent years, we could establish vivid contacts between the networks and learn a lot from each other and together in cooperation. The SonotaCo network provides us with the unique chance to check our findings with an independent dataset, just as we can provide further evidence to findings of the SonotaCo network. For this paper, SonotaCo provided us with the radiant plots (Figure 18 and 19). He confirmed the variation of meteor shower velocities that we detected, and provided fruitful discussions and valuable input for the meteor shower lists.

## References

Arlt R. and Rendtel J. (2006). "A new working list of meteor showers". *WGN, Journal of the IMO*, **36**, 77–84.

Brown P., Weryk R. J., Wong D. K., and Jones J. (2008). "A meteoroid stream survey using the Canadian meteor orbit radar I: Methodology and radiant catalogue". *Icarus*, **195**, 317–339.

Brown P., Wong D. K., Weryk R. J., and Wiegert P. (2009). "A meteoroid stream survey using the Canadian meteor orbit radar II: Identification of minor showers using a 3D wavelet transform". *Icarus*. (submitted).

Dubietis A. and Arlt R. (2002). "The current Delta-Aurigid meteor shower". *WGN, Journal of the IMO*, **30**, 168–174.

Jenniskens P. (2006). *Meteor showers and their parent comets*. Cambridge Univ. Press.

Jenniskens P., Jopek T. J., Rendtel J., Porubčan V., P. P. S., Baggaley J., Abe S., and Hawkes R. (2009). "On how to report new meteor showers". *WGN, Journal of the IMO*, **37**, 19–20.

Jopek T. J. (2009). "IAU Meteor Data Center". `http://www.astro.amu.edu.pl/~jopek/MDC2007` .

Lindblad B. A. (1971). "A computerized stream search among 2401 photographic meteor orbits". *Smithosn. Contr. Astrophys.*, **12**, 14–24.

Molau S. (1998). "The meteor detection software MetRec". In Arlt R., editor, *Proc. IMC 1998, Stara Lesná, Slovakia*, pages 9–16. International Meteor Organization.

Molau S. (2001). "The AKM Video Meteor Network". In Warmbein B., editor, *Proc. Meteoroids 2001, Kiruna, Sweden*, pages 315–318.

Molau S. (2006). "How good is the IMO Working List of meteor showers? A complete analysis of the IMO video meteor database". In Bettonvil F. and Kac J., editors, *Proc. IMC 2006, Roden, the Netherlands*, pages 38–54.

Molau S. (2008). "A new analysis of the IMO video meteor database". In *Proc. IMC 2008, Šachticka, Slovakia*.

Molau S. and Kac J. (2009). "Results of the IMO video meteor network – December 2008". *WGN, Journal of the IMO*, **37**, 43–47.

Molau S. and SonotaCo (2008). "On the average altitude of (video) meteors". *WGN, Journal of the IMO*, **36**, 124–130.

Rendtel J. (1993). "Radiants and orbits of $\delta$-Aurigids and September Perseids". In *Proceedings of the IMC Smolenice 1992*, pages 67–73.

Rendtel J. and Arlt R., editors (2009). *Handbook for meteor observers*. International Meteor Organization.

SonotaCo (2009). "A meteor shower catalog based on video observations in 2007–2008". *WGN, Journal of the IMO*, **37**, 55–62.

*Handling Editor:* Javor Kac

This paper has been typeset from a LaTeX file prepared by the authors.

# Predictions for the 2009 Leonids from a technically dense model

*Esko Lyytinen* [1] *and Markku Nissinen* [2]

We give here our predictions of Leonids for the year 2009. We found two prominent encounters with old trails, from the years 1466 and 1533. Because the 1466 trail gave an outburst in the year 2008 we also update the post prediction of that. It appears that the maximums from these two trails nearly coincide in time, increasing the predicted maximum ZHR for the year 2009 close to 150 if taking the expected annual background also in account. Considering the uncertainties the maximum ZHR might be as high as 300.

## 1 Introduction

The model of Lyytinen,Van Flandern, and Nissinen quite successfully predicted the Leonids storms and outbursts timings and strengths in the years after the parent comet's return in 1998. The general principles of trail modeling were given in: Kondrat'eva & Reznikov (1985); McNaught & Asher (1999); Lyytinen (1999); Lyytinen & Van Flandern (2000); and Lyytinen et al. (2001). The general behaviour of the calculated trails is broadly similar for all these approaches. Lyytinen (1999), Lyytinen & Van Flandern (2000), and Lyytinen et al. (2001) specifically describe the Lyytinen and Van Flandern model.

The model can be considered as two different level models: the basic model and the A-2 model. The basic model is simpler and will give good values for young trails. For older trails non-gravitational "A-2 effects" are expected to have a significant effect and these are taken into account in the more advanced A-2 model. The principles of the basic model and the A-2 model were given in (Lyytinen & Van Flandern, 2000) and (Lyytinen et al., 2001). These references are detailed enough for constructing and applying the model, however, there has been no other work to date using or even testing the A-2 model. The basic model has been in use in a modified form by Maslov (2007) and Maslov (2008).

The A2 effect is a non gravitational effect of radiation forces, that change the orbital periods of meteoroids in each revolution. This is included in the modeling by increasing or decreasing the orbital velocity of the test particles at each perihelion. The applied change is the same at each perihelion for a given particle but differs among the test particle population in general.

In this paper we present the updated comparison of Leonids trail 1466 for the year 2008 and predictions for the year 2009 from trails 1466 and 1533. We also present a prediction for the year 2009 in the case that trails 1466 and 1533 were originally different in density compared to younger trails.

[1]Kehäkukantie 3B, 00720 Helsinki, Finland.
Email: esko.lyytinen@jippii.fi
[2]Kauppakatu 70 A 10, 78200 Varkaus, Finland.
Email: markku.nissinen@pp.inet.fi

IMO bibcode WGN-374-lyytinen-leonids
NASA-ADS bibcode 2009JIMO...37..122L

## 2 General principles

### 2.1 Basic model

The basic model assumes ejections from the parent comet at perihelion with zero ejection velocity. The difference of semi-major axis and orbital period arise from solar radiation pressure. The pressure is considered to be of the basic form, directed away from the Sun and the strength inversely proportional to the square of the distance. The strength is given by $\beta$, which is the ratio of the radiation pressure to the gravitational force at same distance from the Sun. In practical calculations there are a number of test particles with varying values of $\beta$. Typically the number of particles may be about a thousand, which have a fixed spacing in the $\beta$ values. The trail in question is calculated to the desired potential outburst date and a little further. Our program calculates directly the solar distance and solar longitude of the ecliptic plane crossing for the mean ecliptic of the date.

In this model the $\beta$ value is expected to be positive, as it truly is. Most of the observed storms or outbursts have a positive value for $\beta$, but in some instances the actual ejection velocity may make it appear negative. In such a situation the trail passing can be computed by applying a negative $\beta$ value, but one can not get a reasonable ZHR-value from our model in such a case.

The predicted ZHR-curve from one young trail can be calculated with the basic model. The shape along the solar longitude is expected to be a Lorenz curve in this model and the model gives the maximum ZHR value the width and the solar longitude of the maximum.

### 2.2 Non-gravitational model (A-2 model)

The non-gravitational forces are expected to change the orbital period of the meteoroids. We use the term A-2 model, because the A-2 non-gravitational parameter in comet orbits mainly affects the orbital period in each revolution. The reason for the non-gravitational force is different from that of comets but the effect is about the same.

If the meteoroid spin axis stays fixed in space during the orbits from ejection to the outburst, then the orbital period change is the same in each revolution. This is doubtful, but for lack of a better model is a good approximation. This has been applied and the results are well acceptable (Lyytinen et al., 2001). For the orbital period change the velocity is changed at each perihelion. The measure of this change and the corresponding dis-

tribution width is millionths of the true velocity. We do not know the actual distribution shape of this change and lacking a better understanding a Lorenz distribution has been applied. For actual calculations the trail is calculated with different discrete A-2 values.

In principle the ZHR-curve is calculated for each such discrete A-2 value trail and these are added by applying different weights to different A-2 values. The applied weighs are adjusted to correspond with the expected A-2 distribution. As mentioned above, we have adopted the Lorenz distribution for this. Some values for the width of this distribution have been derived in Lyytinen et al. (2001). In this paper we used the half-width of 4.0 (millionths of the true velocity in perihelion) for all the trails.

## 3 Testing the models for the year 2008 and predictions for the year 2009

### 3.1 A dense model for the year 2008 from the trail 1466

In November 2008 an outburst from the trail 1466 was observed with a ZHR of about 110 (IMO, 2008). This outburst was predicted by Vaubaillon (2008) and Maslov (2008). Prior to the 2008 Leonids we also calculated a predicted Leonids ZHR of 20 (which we did not publish). A later examination seems to reveal the reason for this low value. In the trail there was a very dense grouping. This grouping was very short in time and only about one day before our selected "pick window" for the model meteoroids taken into account.

The pick window is a time span centered on the predicted time of the shower, from which we take the needed statistical data of the test particles. Because the number of test particles can not be especially large, the pick window needs to be much longer than the actual duration of the shower to get a big enough sample of the test particles. The pick window is typically a few days.

Applying the A-2 effect shifted the grouping in time over this window but too quickly for the calculated discrete A-2 value trails. The grouping practically skipped over the pick window and as a result failed to make its proper statistical contribution to the results. Therefore we now create a more dense model, in the sense of a denser sampling in A-2 space. We emphasize that this dense model does not mean any artificial increase of meteoroids in the stream.

Thus we have now made a denser model, as regards the applied A2 values. In this we paid special attention that this group had the proper effect as to the size of the pick window and the movement of it with changing A2 value. The result is given in Figure 1. This has the maximum ZHR of 46. Combined with an expected background of about 20 this would be ∼65. This is still below the observed ZHR, but a fit within a factor 2 is considered good enough. Perhaps this old trail was originally denser than typical for more young trails. The maximum is at solar longitude 234.°96. The observed maximum was at 234.°974 (IMO, 2008). Our original prediction gave this earlier in time and this more elaborate prediction has a better fit also in this.

### 3.2 Predictions for the year 2009 from the trails 1466 and 1533

We used the denser, in A2 range, than typical trail calculations of the trail 1466 also for the year 2009. It however appears that there would practically be no need for denser than normal modeling. The prediction from the trail 1533 is calculated with the normal A2 value density. The results are given in Figures 2 and 3.

Both of these have the maximum ZHR of about 60. The solar longitudes about coincide, and the combined maximum is the sum of these, about 120. The normal background of about 20 should be added to this. So the predicted total maximum ZHR value is expected to be about 145. If the 1466 trail was originally denser than the presently younger trails were originally, then an even stronger maximum is expected.

Further, there may be the possibility that the trails in general have became more weak because of the aging of the parent comet, and also the 1533 trail ZHR should be multiplied by maybe twofold, because that factor gives the correct ZHR for the 1466 trial in 2008. This would give the combined ZHR possibly as high as 260. Of course typical prediction errors or inaccuracies can further affect to this.

The combined maximum is expected to occur at solar longitude 235.°535. This is on November 17 at $21^{\mathrm{h}}28^{\mathrm{m}}$ UT. The result is given at Figure 4. Trails other than 1466 and 1533 do not affect predicted ZHR for year 2009 significantly in our model.

## 4 Discussion

The year 2009 appears to be a good year for the Leonids. There are not many strong predicted meteor outbursts in the near future, maybe not until near the next Leonids parent comet return. So the 2009 outbursts are important in validating and further developing the prediction methods. Predictions for this year's shower have also been made by Vaubaillon (2009), using the Vaubaillon (2002) and Vaubaillon et al. (2005) model.

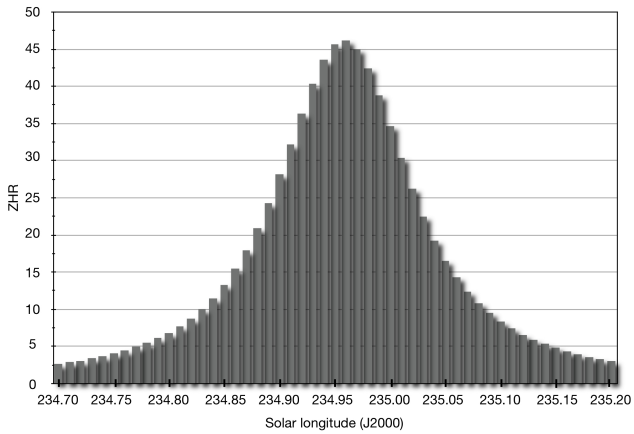


*Figure 1* – Post prediction for the year 2008 from the trail 1466.

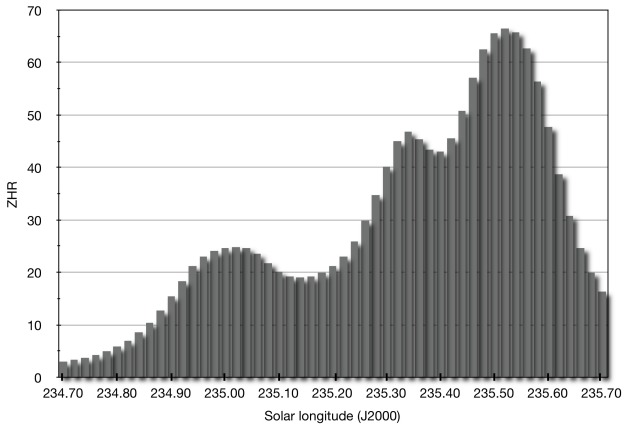


*Figure 2* – Prediction for the year 2009 from the trail 1466.

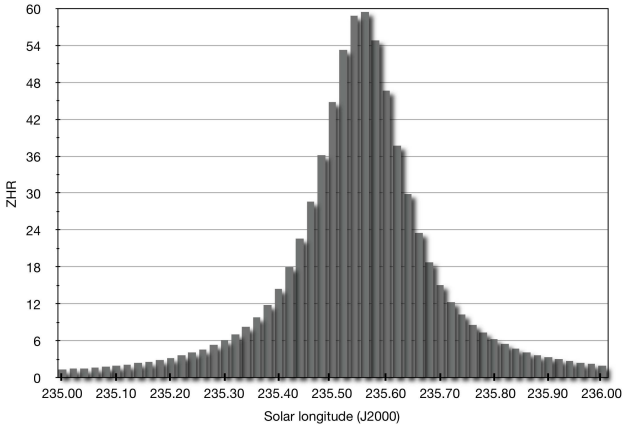


*Figure 3* – Prediction for the year 2009 from the trail 1533.

The observed outburst from trail 1466 observed in November 2008 may indicate that the trail 1466 could be denser than younger trails. The general accuracy of the maximum ZHR predictions during the Leonid storms seems to have been relatively within about a factor of 2. The discrepancy of the 1466 in 2008 is about this level, so we cannot make any reliable conclusions about the trails original strength. This may have been stronger than typical and/or the old trails in general could have been stronger than more recent trails. There is the possibility that the 1466 trail in 2009 will produce a maximum ZHR about two times predicted here. The maximum combined ZHR for the 1466 and 1533 trails might be as high as about 260 (rounded to 300).

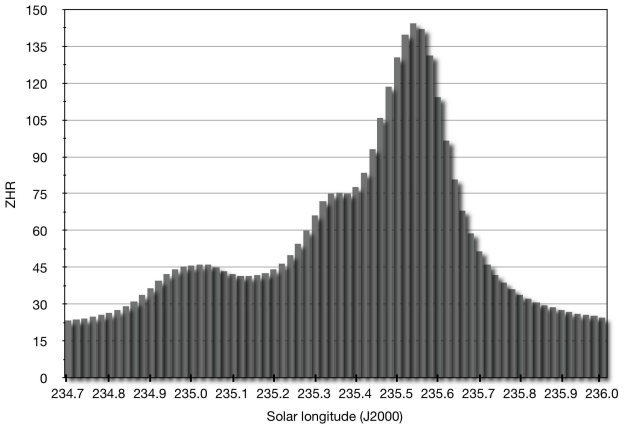


*Figure 4* – Prediction for the year 2009 from trails 1533 and 1466 with annual component.

## References

IMO (2008). "Leonids 2008: visual data quicklook". `http://www.imo.net/live/leonids2008` . International Meteor Organization website.

Kondrat'eva E. D. and Reznikov E. A. (1985). "Comet Tempel-Tuttle and the Leonid meteor swarm". *Sol. System Res.*, **19**, 96–101.

Lyytinen E. (1999). "Leonid predictions for the years 1999-2007 with the satellite model of comet". *Meta Research Bulletin*, **8**, 33–40.

Lyytinen E., Nissinen M., and Van Flandern T. (2001). "Improved 2001 Leonid storm predictions from a refined model". *WGN*, **29:4**, 110–118.

Lyytinen E. and Van Flandern T. (2000). "Predicting the strength of Leonid outbursts". *Earth, Moon and Planets*, **82-83**, 149–166.

Maslov M. (2007). "Leonid predictions for the period 2001-2100". *WGN*, **35:1**, 5–12.

Maslov M. (2008). "Leonids 2001-2010". `http://feraj.narod.ru/Radiants/Predictions/1901-2100eng/Leo2001-2010eng.html` .

McNaught R. H. and Asher D. J. (1999). "Leonid dust trails and meteor storms". *WGN*, **27:2**, 85–102.

Vaubaillon J. (2002). "Activity level prediction for the 2002 Leonids". *WGN*, **30:5**, 144–148.

Vaubaillon J. (2008). "(Earth) 2008 Leonids". `http://www.imcce.fr/en/ephemerides/phenomenes/meteor/DATABASE/Leonids/2008` .

Vaubaillon J. (2009). "2009 Leonids". `http://www.imcce.fr/en/ephemerides/phenomenes/meteor/DATABASE/Leonids/2009` .

Vaubaillon J., Colas F., and Jorda L. (2005). "A new method to predict meteor showers, II: Application to Leonids". *Astronomy & Astrophysics*, **439**, 761–770.

*Handling Editor:* John Correira

# Preliminary results

## Results of the IMO Video Meteor Network — May 2009

*Sirko Molau* [1] *and Javor Kac* [2]

The meteor activity in all 31 nights of 2009 May was covered by the IMO Video Meteor Network cameras. In almost exactly 2000 hours of effective observing time, 32 cameras recorded almost 4800 meteors. $\eta$-Aquariids and $\eta$-Lyrids were both captured well by the cameras. Their radiant drifts and activity profiles are presented.

Received 2009 June 26

### 1 Introduction

The weather in May was not record-breaking, but better than average. Twelwe out of 32 cameras recorded meteors in 20 or more nights, and in total we collected almost exactly 2 000 hours of effective observing time (Table 1). The 5 000 recorded meteors are in particular valuable, because most observers suffer from the short northern hemisphere nights and the low overall activity at that time of year (Figure 1). Thus, May and June are still the months with the smallest overall data set.

Looking at the list of meteor showers in May, we find with the $\eta$-Aquariids the strongest source of the southern hemisphere, and with the $\eta$-Lyrids a minor shower that was only in 2007 included into the IMO meteor shower list (Arlt & Rendtel, 2006), beside the always active antihelion source. From the analysis perspective, the $\eta$-Aquariids are particularly interesting. At the mid-northern latitudes, where most video observers are currently active, they are hardly to observe because the radiant rises only shortly before sunrise. Typically one will catch only a handful of shower members at dawn of the shower maximum. When the observability function is applied to correct for the observing geometry, each $\eta$-Aquariid observed at 48° N gets a weight of 30 — that is about twenty times as much weight as a Geminid in mid-December would get. Hence, only small scatter or systematic deviations will have a tremendous impact on the meteor shower activity. Still, the obtained activity profile gives quite a consistent picture.

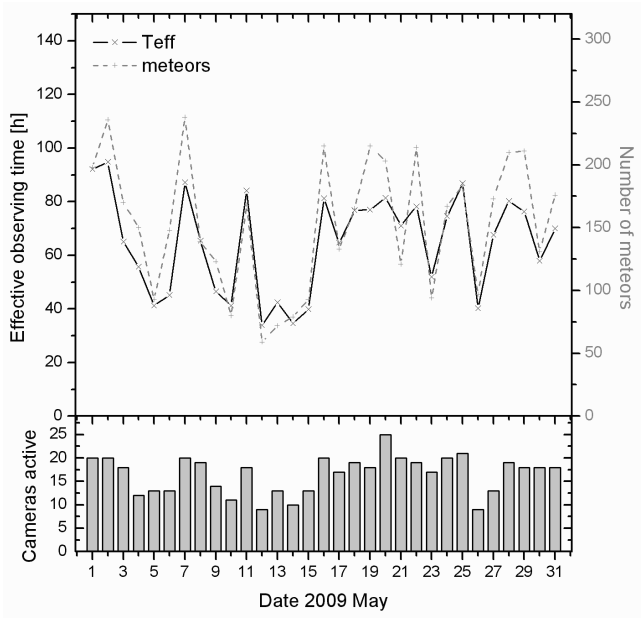


*Figure 1* – Monthly summary for the effective observing time (solid black line), number of meteors (dashed gray line) and number of cameras active (bars) in 2009 May.

### 2 $\eta$-Aquariids

The meteor shower analysis presented at the 2008 IMC (Molau, 2009) revealed an activity interval of the $\eta$-Aquariids between April 27 and May 18, based on a thousand shower members (Figure 2). The interval is clearly shorter than the one given in the IMO working list, but the activity is above ten between April 28 and May 15. That hints on possible extended meteor shower activity beyond the limits given here. The determined meteor shower velocity of 67 km/s agrees well with the value from literature (66 km/s) and also the radiant position is confirmed by our video observations. Only the amount of the radiant drift is smaller than expected.

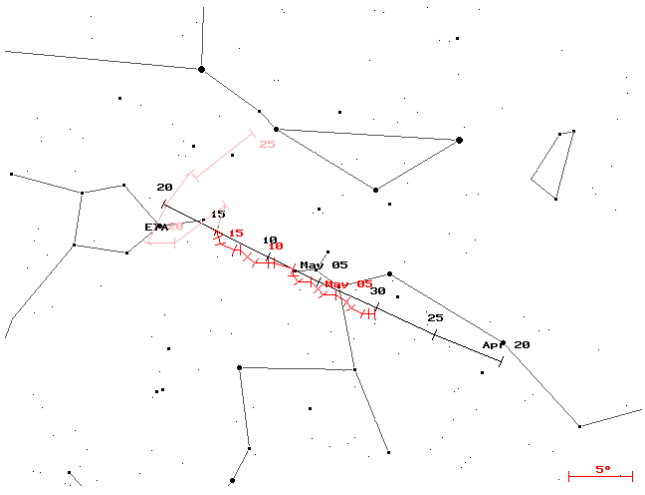


*Figure 2* – Radiant position of the $\eta$-Aquariids from data of the IMO Video Meteor Database. Black line denotes the radiant drift of the shower as given in the IMO Handbook (Rendtel & Arlt, 2008).

[1] Abenstalstr. 13b, 84072 Seysdorf, Germany.
Email: sirko@molau.de
[2] Na Ajdov hrib 24, 2310 Slovenska Bistrica, Slovenia.
Email: javor.kac@orion-drustvo.si

IMO bibcode WGN-374-molau-vidmay
NASA-ADS bibcode 2009JIMO...37..125M

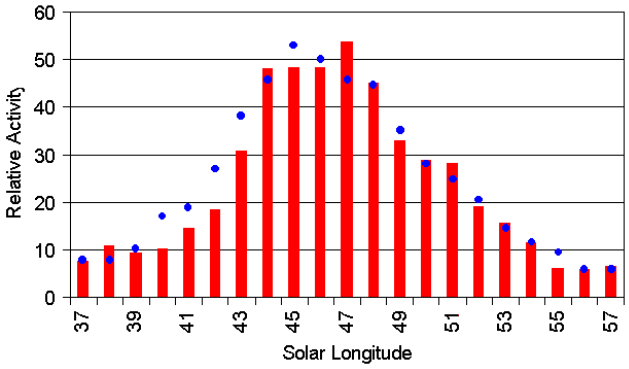


*Figure 3* – Long-term activity profile of the $\eta$-Aquariids. Dots present the ZHR profile obtained from visual data.

Figure 3 depicts the activity profile of the $\eta$-Aquariids. The dots represent the long-term activity profile obtained from visual observations, averaged over two degrees solar longitude. Both graphs match remarkably well, in particular if the large correction factors are taken into consideration. According to the video data, the maximum occurs at 47° solar longitude, about 1.5 days later than in the visual data. However, there is a plateau of high activity early May, which is why the time of maximum may vary easily.

## 3 $\eta$-Lyrids

The $\eta$-Lyrids, the second shower of May, can be identified between May 7 and 14 based on 260 shower members. Their activity interval starts later but last also somewhat longer than given in the IMO meteor shower list. The radiant position (Figure 4) agrees well with the value from literature, but there is no clear radiant drift in the full activity interval. It rather seems that the radiant is stationary. The velocity of 43 km/s determined from the video data agrees once more well with the value from the IMO meteor shower list (44 km/s).

The activity profile (Figure 5) is symmetric and reaches a maximum of about 2 at May 11. The IMO handbook gives a value of three around May 8 (Rendtel & Arlt, 2008). However, at such low rates the maximum date derived from video data is more reliable. Also here we may have another look at the observability function: As the $\eta$-Lyrid radiant is high in the sky all night long, the correction factor is one order of magnitude smaller than that of the $\eta$-Aquariids. That reflects also in the plain meteor counts. Even though their activity interval is more than twice as long and the maximum rate even a factor of 25 higher, the total number of $\eta$-Aquariids recorded so far is only a factor of four larger than the number of $\eta$-Lyrids.

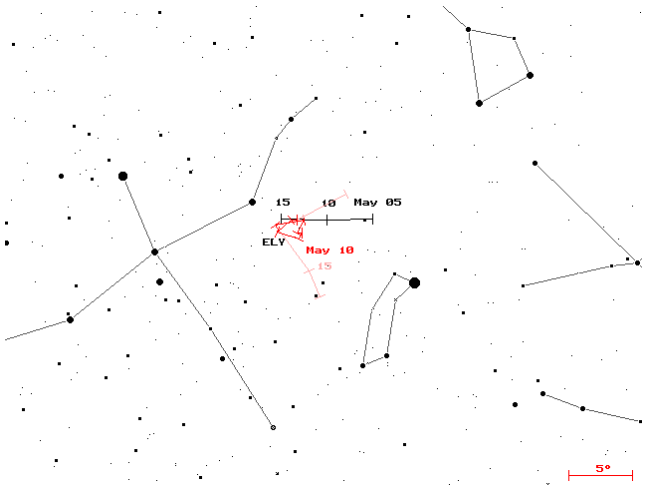


*Figure 4* – Radiant position of the $\eta$-Lyrids from data of the IMO Video Meteor Database. Black line denotes the radiant drift of the $\eta$-Lyrids as given in the IMO Handbook (Rendtel & Arlt, 2008).

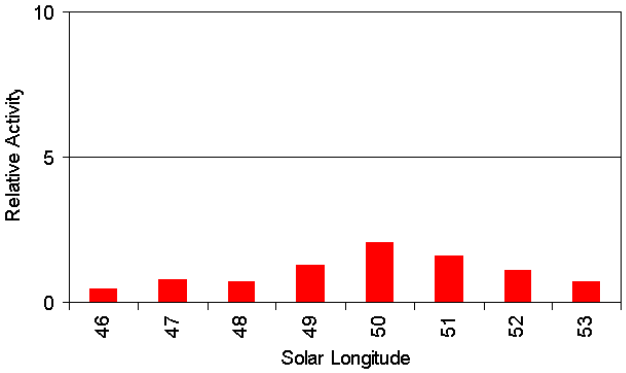


*Figure 5* – Long-term activity profile of the $\eta$-Lyrids.

## References

Arlt R. and Rendtel J. (2006). "A new Working List of meteor showers". *WGN*, **34:4**, 77–84.

Molau S. (2009). "A new analysis of the IMO video meteor database". In *Proceedings of the International Meteor Conference*, Šachtička, Slovakia, September 18-21, 2008. International Meteor Organization. (in press).

Rendtel J. and Arlt R. (2008). *Handbook for meteor observers*. International Meteor Organization, Potsdam.

*Handling Editor:* Javor Kac

*Table 1* – Observers contributing to May 2009 data of the IMO Video Meteor Network.

| Code | Name | Place | Camera | FOV | LM | Nights | Time (h) | Meteors |
|---|---|---|---|---|---|---|---|---|
| BENOR | Benitez-S. | Las Palmas | TIMES5 (0.95/50) | ⊘ 10° | 3 mag | 3 | 4.9 | 6 |
| BRIBE | Brinkmann | Herne | HERMINE (0.8/6) | ⊘ 55° | 3 mag | 25 | 72.3 | 214 |
| CASFL | Castellani | Monte Baldo | BMH1 (0.8/6) | ⊘ 55° | 3 mag | 18 | 42.6 | 82 |
| | | | BMH2 (0.8/6) | ⊘ 55° | 3 mag | 19 | 62.3 | 96 |
| CRIST | Crivello | Valbrevenna | C3P8 (0.8/3.8) | ⊘ 80° | 3 mag | 27 | 141.8 | 340 |
| ELTMA | Eltri | Venezia | MET38 (0.8/3.8) | ⊘ 80° | 3 mag | 3 | 9.5 | 17 |
| GONRU | Goncalves | Tomar | TEMPLAR1 (0.8/6) | ⊘ 55° | 3 mag | 22 | 144.7 | 414 |
| | | | TEMPLAR2 (0.8/6) | ⊘ 55° | 3 mag | 22 | 100.2 | 230 |
| GOVMI | Govedič | Središče ob Dravi | ORION2 (0.8/8) | ⊘ 42° | 4 mag | 12 | 59.1 | 169 |
| HERCA | Hergenrother | Tucson | SALSA (1.2/4) | ⊘ 80° | 3 mag | 26 | 133.9 | 195 |
| HINWO | Hinz | Brannenburg | AKM2 (0.85/25) | ⊘ 32° | 6 mag | 12 | 42.3 | 103 |
| IGAAN | Igaz | Hódmező-vásárhely | HUHOD (0.8/3.8) | ⊘ 80° | 3 mag | 18 | 80.6 | 139 |
| JOBKL | Jobse | Oostkapelle | BETSY2 (1.2/85) | ⊘ 25° | 7 mag | 16 | 67.2 | 303 |
| KACJA | Kac | Kostanjevec | METKA (0.8/8) | ⊘ 42° | 4 mag | 15 | 42.2 | 55 |
| | | Ljubljana | ORION1 (0.8/8) | ⊘ 42° | 4 mag | 21 | 73.2 | 110 |
| | | Kamnik | REZIKA (0.8/6) | ⊘ 55° | 3 mag | 12 | 60.6 | 187 |
| | | | STEFKA (0.8/3.8) | ⊘ 80° | 3 mag | 11 | 33.0 | 42 |
| LUNRO | Lunsford | Chula Vista | BOCAM (1.4/50) | ⊘ 60° | 6 mag | 7 | 14.1 | 106 |
| MOLSI | Molau | Seysdorf | AVIS2 (1.4/50) | ⊘ 60° | 6 mag | 11 | 46.0 | 398 |
| | | | MINCAM1 (0.8/6) | ⊘ 60° | 3 mag | 20 | 56.6 | 105 |
| | | Ketzür | REMO1 (0.8/3.8) | ⊘ 80° | 3 mag | 25 | 90.8 | 136 |
| | | | REMO2 (0.8/3.8) | ⊘ 80° | 3 mag | 25 | 102.5 | 229 |
| OCHPA | Ochner | Albiano | ALBIANO (1.2/4.5) | ⊘ 68° | 3 mag | 24 | 80.2 | 141 |
| PRZDA | Przewozny | Berlin | ARMEFA (0.8/6) | ⊘ 55° | 3 mag | 10 | 42.7 | 84 |
| SLAST | Slavec | Ljubljana | KAYAK1 (1.8/28) | ⊘ 50° | 4 mag | 18 | 58.7 | 85 |
| STOEN | Stomeo | Scorze | MIN38 (0.8/3.8) | ⊘ 80° | 3 mag | 22 | 116.5 | 277 |
| | | | NOA38 (0.8/3.8) | ⊘ 80° | 3 mag | 8 | 36.3 | 48 |
| | | | SCO38 (0.8/3.8) | ⊘ 80° | 3 mag | 21 | 101.5 | 270 |
| STRJO | Strunk | Herford | MINCAM2 (0.8/6) | ⊘ 55° | 3 mag | 19 | 34.6 | 60 |
| | | | MINCAM3 (0.8/8) | ⊘ 42° | 4 mag | 7 | 12.3 | 24 |
| | | | MINCAM5 (0.8/6) | ⊘ 55° | 3 mag | 11 | 29.1 | 71 |
| YRJIL | Yrjölä | Kuusankoski | FINEXCAM (0.8/6) | ⊘ 55° | 3 mag | 4 | 14.3 | 19 |
| | | | | | Overall | 31 | 2 006.6 | 4 755 |

# Results of the IMO Video Meteor Network — June 2009

*Sirko Molau* [1] *and Javor Kac* [2]

The 2009 June IMO Video Meteor Network results are presented. All nights were covered by the observations from 34 cameras. More than 3 600 meteors were recorded in about 1 400 hours effective observing time. The N Apex radiant drift is presented.

Received 2009 July 28

## 1 Introduction

June presented to the observers not only short nights, but often also poor weather. The start of Summer was not really noticeable in many parts of Europe, and our American observers suffered from unusually poor weather, too. So it comes as no surprise that just three cameras managed to observe in 20 or more nights. That is a pity, because June has become the month with least data. Still, thanks to more than 3 000 meteors of 2009, the total number of June meteors in the IMO Video Meteor Database has increased to 18 000 (Table 1 and Figure 1). That is about a quarter of the meteor number from the best month (October). Furthermore, June marks finally the end of the spring meteor activity minimum. According to the long-term statistics, the hourly meteor rate recorded by our cameras increases from 2.4 on average in May to 3.0 in June. It will further increase to 4.7 in July and finally reach the annual maximum of 7.2 meteors per hour thanks to the Perseids in August.

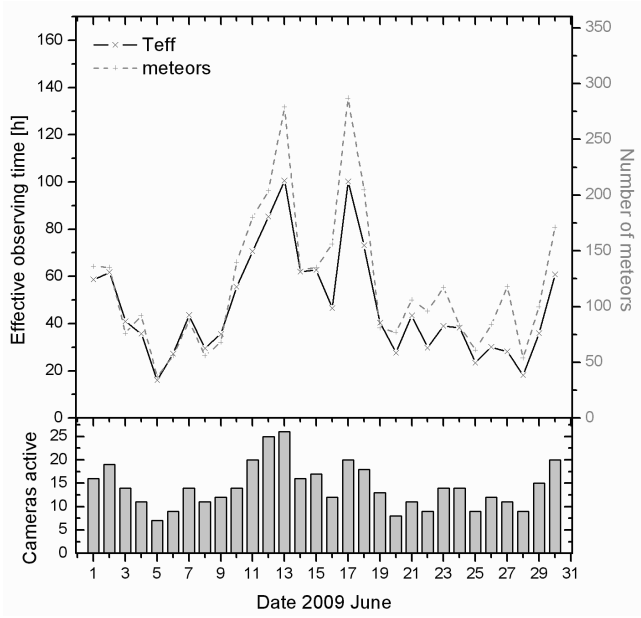


*Figure 1* – Monthly summary for the effective observing time (solid black line), number of meteors (dashed gray line) and number of cameras active (bars) in 2009 June.

## 2 Nortern Apex meteors

Looking at the IMO shower list (Arlt & Rendtel, 2006), there is no shower besides the June Bootids. These are only occasionally active and were not recognized as an independent shower. Looking at the radiant lists from individual solar longitudes, they show up only sometimes. On the other hand, the N Apex is a remarkably prominent sporadic source in June. The radiant can be tracked from June 18 till July 30, when it moves from Pegasus to Triangulum (Figure 2). The scatter of the radiant position is stronger than for a usual shower, which should not surprise. After all, that is not a real meteor shower with a well defined radiant, but only a diffuse radiation area.

The high velocity of 68 km/s on average is typical for an Apex source. The activity profile (Figure 3) is relatively flat with a rate of four. Thus, the N Apex source in June is clearly more active than some of the minor showers in the IMO working list!

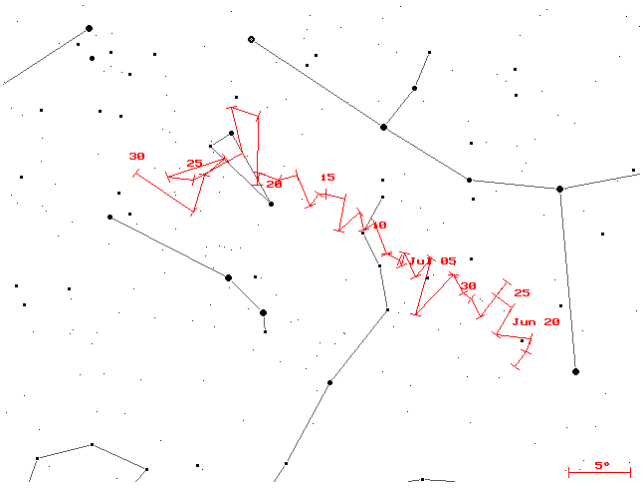


*Figure 2* – Radiant position of the N Apex source in June/July obtained from data of the IMO Video Meteor Database.

## References

Arlt R. and Rendtel J. (2006). "A new Working List of meteor showers". *WGN*, **34:4**, 77–84.

[1]Abenstalstr. 13b, 84072 Seysdorf, Germany.
Email: sirko@molau.de
[2]Na Ajdov hrib 24, 2310 Slovenska Bistrica, Slovenia.
Email: javor.kac@orion-drustvo.si

*Handling Editor:* Javor Kac

IMO bibcode WGN-374-molau-vidjun
NASA-ADS bibcode 2009JIMO...37..128M

*Table 1* – Observers contributing to June 2009 data of the IMO Video Meteor Network.

| Code | Name | Place | Camera | FOV | LM | Nights | Time (h) | Meteors |
|---|---|---|---|---|---|---|---|---|
| BENOR | Benitez-S. | Las Palmas | TIMES5 (0.95/50) | ⊘ 10° | 3 mag | 8 | 28.9 | 47 |
| BRIBE | Brinkmann | Herne | HERMINE (0.8/6) | ⊘ 55° | 3 mag | 15 | 40.2 | 119 |
| CASFL | Castellani | Monte Baldo | BMH1 (0.8/6) | ⊘ 55° | 3 mag | 16 | 43.4 | 109 |
| | | | BMH2 (0.8/6) | ⊘ 55° | 3 mag | 16 | 39.8 | 79 |
| CRIST | Crivello | Valbrevenna | C3P8 (0.8/3.8) | ⊘ 80° | 3 mag | 18 | 65.6 | 186 |
| | | | STG38 (0.8/3.8) | ⊘ 80° | 3 mag | 1 | 4.1 | 14 |
| ELTMA | Eltri | Venezia | MET38 (0.8/3.8) | ⊘ 80° | 3 mag | 6 | 28.0 | 66 |
| GONRU | Goncalves | Tomar | TEMPLAR1 (0.8/6) | ⊘ 55° | 3 mag | 19 | 103.3 | 334 |
| | | | TEMPLAR2 (0.8/6) | ⊘ 55° | 3 mag | 21 | 77.8 | 171 |
| GOVMI | Govedič | Središče ob Dravi | ORION2 (0.8/8) | ⊘ 42° | 4 mag | 19 | 87.4 | 277 |
| HERCA | Hergenrother | Tucson | SALSA (1.2/4) | ⊘ 80° | 3 mag | 22 | 72.6 | 97 |
| | | | SALSA2 (1.2/4) | ⊘ 80° | 3 mag | 18 | 64.5 | 93 |
| HINWO | Hinz | Brannenburg | AKM2 (0.85/25) | ⊘ 32° | 6 mag | 8 | 15.8 | 42 |
| IGAAN | Igaz | Hódmező-vásárhely | HUHOD (0.8/3.8) | ⊘ 80° | 3 mag | 14 | 64.9 | 104 |
| JOBKL | Jobse | Oostkapelle | BETSY2 (1.2/85) | ⊘ 25° | 7 mag | 11 | 39.2 | 167 |
| KACJA | Kac | Kostanjevec | METKA (0.8/8) | ⊘ 42° | 4 mag | 13 | 51.6 | 74 |
| | | Ljubljana | ORION1 (0.8/8) | ⊘ 42° | 4 mag | 20 | 55.0 | 85 |
| | | Kamnik | REZIKA (0.8/6) | ⊘ 55° | 3 mag | 9 | 33.3 | 94 |
| | | | STEFKA (0.8/3.8) | ⊘ 80° | 3 mag | 6 | 15.6 | 24 |
| KOSDE | Koschny | Noord-wijkerhout | TEC1 (1.4/12) | ⊘ 30° | 4 mag | 6 | 21.0 | 36 |
| LUNRO | Lunsford | Chula Vista | BOCAM (1.4/50) | ⊘ 60° | 6 mag | 5 | 19.4 | 83 |
| MOLSI | Molau | Seysdorf | AVIS2 (1.4/50) | ⊘ 60° | 6 mag | 9 | 23.5 | 218 |
| | | | MINCAM1 (0.8/6) | ⊘ 60° | 3 mag | 17 | 49.5 | 85 |
| | | Ketzür | REMO1 (0.8/3.8) | ⊘ 80° | 3 mag | 11 | 21.3 | 46 |
| | | | REMO2 (0.8/3.8) | ⊘ 80° | 3 mag | 12 | 24.9 | 73 |
| OCHPA | Ochner | Albiano | ALBIANO (1.2/4.5) | ⊘ 68° | 3 mag | 3 | 13.3 | 37 |
| PRZDA | Przewozny | Berlin | ARMEFA (0.8/6) | ⊘ 55° | 3 mag | 6 | 17.7 | 48 |
| SLAST | Slavec | Ljubljana | KAYAK1 (1.8/28) | ⊘ 50° | 4 mag | 14 | 34.9 | 63 |
| STOEN | Stomeo | Scorze | MIN38 (0.8/3.8) | ⊘ 80° | 3 mag | 17 | 71.9 | 247 |
| | | | NOA38 (0.8/3.8) | ⊘ 80° | 3 mag | 15 | 51.1 | 104 |
| | | | SCO38 (0.8/3.8) | ⊘ 80° | 3 mag | 15 | 70.4 | 211 |
| STRJO | Strunk | Herford | MINCAM2 (0.8/6) | ⊘ 55° | 3 mag | 15 | 24.2 | 44 |
| | | | MINCAM3 (0.8/8) | ⊘ 42° | 4 mag | 8 | 14.2 | 30 |
| | | | MINCAM5 (0.8/6) | ⊘ 55° | 3 mag | 13 | 32.8 | 103 |
| | | | | | Overall | 30 | 1 421.1 | 3 610 |

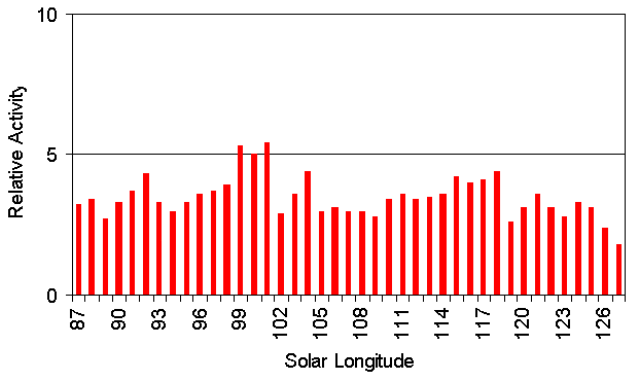


*Figure 3* – Long-term activity profile of the N Apex source in June/July.

# History

## Meteor Beliefs Project: The Tauric Artemis in Classical times

*Alastair McBeath*[1] *and Andrei Dorian Gheorghe*[2]

A discussion of the supposedly sky-fallen statue of the deity Tauric Artemis is presented, as described in texts from the Classical period of European history. The widespread nature of claims for where the statue was preserved after its removal from the Crimean Peninsula, suggest it was an unusually significant, potentially meteoritic, object.

Received 2009 June 13

### 1 Introduction

When we last discussed the worship of what were claimed as objects fallen from the heavens in the Classical world (McBeath & Gheorghe, 2005), we ran out of space and time to include one further notable example, that of the statue of the Tauric Artemis. We have redressed that omission here. The objects in that earlier article, and the Palladium, which we also examined previously (McBeath & Gheorghe, 2004), were said to have been worshipped at a primary site where they fell, or were removed to a specific secondary place to be revered. The Tauric Artemis began that way too, but it ended up with a list of secondary worship sites that spanned half the known Classical world, from Italy east to modern western Iran, without any of these locations seeming to have had an overall predominance, or a definitive claim to ownership of the original statue.

### 2 A sky-fallen image

The earliest surviving mention of the celestial origins of the Tauric Artemis was from ancient Greece, in Euripides' play "Iphigenia in Taurica". Euripides lived and wrote in the 5th century BC, and it has been conjectured that he wrote this play towards the end of his life, around 414–412 BC (Way, 1912, pp. x–xii; Euripides died in 406 BC). The key passage came in lines 85–88, spoken by Iphigenia's brother Orestes, and addressed to the unseen god Apollo:

"Thou bad'st me go unto the Taurian coasts Where Artemis thy sister hath her altars, And take the Goddess' image, which, men say, Here fell into this temple out of heaven"

(Way, 1912, pp. 290–291, lines 85–88).

Euripides in this passage used a phrasing with the term 'ouranos' for the 'fell out of heaven' line, though elsewhere, he employed 'diopetes' (e.g. line 978, op. cit., pp. 362–363) or 'ouranos' apparently interchangeably in such matters (e.g. line 986, loc. cit.). On the significance of both terms in relation to ancient Greek descriptions of potential meteorites, see (McBeath & Gheorghe, 2005). However, rather like the Palladium and some of the other Classical objects thought to have dropped from the sky, the Tauric Artemis was made of wood, according to VI.26 of the "Epitome" to Apollodorus' "Library" (Frazer, 1921, pp. 272–273; probably dated to the 1st or 2nd century AD). Whether this meant the original object was wooden, or that a duplicate in wood was made later, cannot be established, though the widespread nature of locations claiming to have had the original statue suggested some copies may indeed have been prepared. If so, this could have implications for the wooden Palladium also being a copy of perhaps an originally genuine meteorite.

No full description of the statue's appearance seems to have survived, though it was clear it must have been relatively small and readily portable. For instance, in various texts, including Euripides' play, both Iphigenia and Orestes handled and carried it with little effort. This too was reminiscent of the portable nature of the Palladium, and the small Magna Mater stone, as described by Arnobius of Sicca (McBeath & Gheorghe, 2005, p. 137).

### 3 The perceived power of the statue

Regardless of the credence given to Euripides' version of events, where the image fell directly into the temple of Artemis, Classical sources agreed that this temple was in the Tauric Chersonese, modernly the Crimean peninsula of Ukraine (see Figure 1), sometimes with parts of the adjacent Black Sea and Sea of Azov coasts, ancient Scythia. The temple's location was not given more precisely than this.

During the 8th to 6th centuries BC, as part of a general expansion in contacts beyond their homeland, the ancient Greeks established a few trading colonies on the southern Crimea, and at least nominally controlled parts of the coast here and nearby from other colonies for trade purposes. By the 1st century AD, the Crimea and all the Black Sea and Sea of Azov coasts were considered part of the Roman Empire. However, this region remained at the dangerous edge of the known world in the minds of the Classical-period Mediterranean civilizations.

Herodotus, like Euripides, writing in the 5th century BC ("Histories", IV.103; Rawlinson, 1996, p. 341), noted the inhabitants of Taurica sacrificed prisoners of war, anyone shipwrecked on their coasts, and all Greeks forced into their ports by the weather, to the virgin god-

[1]12a Prior's Walk, Morpeth, Northumberland, NE612RF, England, UK. Email: meteor@popastro.com

[2]Bd. Tineretului 53, bl. 65, ap. 40, sect. 4, Bucureşti, Romania. Email: agdsarm@gmail.com

IMO bibcode WGN-374-mcbeath-artemis
NASA-ADS bibcode 2009JIMO...37..130M

dess Iphigenia, striking them with a club, and flinging their bodies, or sometimes just their severed heads, over a cliff (if the latter, then burying the headless corpses). The heads might be otherwise fixed onto tall poles, and mostly placed above house-chimneys. Euripides and, drawing on his writings, Apollodorus (cf. Frazer, 1921, pp. 272–273, including Footnotes 2 & 3) instead described the sacrificed corpses as cast into the sacred fires in the temple, which came up through a rock from the subterranean depths of Hades. As described then, this temple was established in Greek thought as a substantial place at the heart of Tauric society.

Other than Herodotus though, the remaining Classical authors who described events surrounding the statue, gave the virgin goddess' name as Artemis, with Iphigenia as her high-priestess, possibly in an attempt to fix a foreign deity within their own pantheon. In the more internally-consistent version (there are others; cf. Graves, 1992, myth 112), Iphigenia and Orestes were two of Clytemnestra and Agamemnon's children, Agamemnon the leader of the Greeks at Troy. Iphigenia became high-priestess in Taurica by magical means. She was to have been sacrificed to answer a prophecy and release the Greek fleet on its way to Troy, windbound at Aulis on the eastern Greek mainland just north of Attica. Artemis was said to have saved her, having provided an animal substitute, and whisked her away to the Tauric Chersonese wrapped in a cloud. Presumably, this method of arrival persuaded the Tauricans to adopt her as their priestess, the only person allowed to handle the sacred, celestial image, rather than, as usual, simply sacrificing her to their deity. (This condenses information from a number of ancient sources. See op. cit., myths 104, 112, 116 & 161 for reference pointers.)

During Agamemnon's ten-year absence at the siege of Troy, Aegisthus, who had not joined the Greek army there, became Clytemnestra's lover, and plotted with her to kill Agamemnon on his return, which they did. Orestes later killed them both in revenge. However, Orestes was driven mad afterwards by the monstrous Erinnyes, the ancient Greeks' personified pangs of guilt and conscience (on all this, cf. op. cit., myths 112–114). At the oracle of Apollo at Delphi, as we saw in the quotation from Euripides above, Orestes was told he could be freed of his madness by retrieving the Tauric Artemis statue.

When Orestes reached the Tauric Chersonese, he was captured and taken before King Thoas, who sent him to the temple to be sacrificed. As detailed in Euripides' play, Iphigenia recognised Orestes, and the two planned to escape back to Greece by boat with the image. Iphigenia convinced the king Orestes was a matricide, and thus needed to be purified by sea water at the coast, together with the statue, before he could be sacrificed. She cited in support that the statue had turned from its place of its own accord, and closed its eyes (Way, 1912, pp. 378–379, lines 1165–1167), and further persuaded the king that no one from the city must see them on their way, or at the shore, while the king was tasked to purify the temple with fire in her absence. So Orestes and his sister made their escape, and he was freed of the Erinnyes.

## 4 A well-travelled idol

Euripides' play had Orestes and Iphigenia return with the Tauric Artemis to Athens, from where it was taken to a purpose-built temple elsewhere in Attica, at the unknown place Halae. There it was known as Artemis Tauropolus or Brauronian Artemis. It still received human blood sacrifices, but not to the extent of killings. Apollodorus though ("Epitome", VI.27; Frazer, 1921, pp. 274–275) seemed to suggest the image was to remain in Athens, and that it was still present there in his time, called Tauropolus. In his "Description of Greece", Pausanias (circa 120–180 AD) referred to a sanctuary of Brauronian Artemis on the Acropolis at Athens as still present then, but he particularly mentioned the image in it was a more recent one by the artist Praxiteles, not the original from Taurica (Book I, XXIII.7; Jones, 1918, pp. 116–119). Pausanias continued unambiguously that the Tauric Artemis itself was preserved at Brauron, on the eastern side of the Attic peninsula, almost opposite Athens on the west coast.

Later in Book I (XXXIII.1; op. cit., pp. 178–179), Pausanias noted Iphigenia had landed at Brauron after escaping from Taurica, and left the Artemis image there instead. He also contradicted his earlier statement by writing that this was actually bf not the original idol, as the earlier wooden statue was at a place sacred to Artemis Orthia called Limnaeum at Lacedaemon (= Sparta), on the Laconian peninsula of southern Greece. He presented in support much 'evidence', including that human blood was used in the ceremonies there, albeit from scourging, rather than full sacrifices. In one of the few notes on the image's appearance, he said the priestess held the small, light, wooden idol nearby, while these rituals were performed. He continued that if the scourging was not vigorously applied, the statue grew so heavy, the priestess could scarcely carry it, in a further attempt to indicate the power of its magical properties as the 'true' image. See Book III, XVI.7 & 9–11 (Jones & Ormerod, 1926, pp. 100–103).

In Book III, XVI.8, Pausanias reported the then-current alternative claims for the 'true' image to have been with the Cappadocians, or the Lydians at their sanctuary of Artemis Anaeitis, both in parts of modern Turkey. He mentioned though that these were "the Cappadocians dwelling on the Euxine", the meaning of which is unclear, because 'the Euxine' was the Black Sea, whereas various ancient authors confirmed the Cappadocian territories as well south of the Black Sea coasts. Pausanias may have intended a different area than that shown in Figure 1 here, perhaps the lands of one of the coastal peoples of the southern Black Sea, which were, in order moving east from the Bosporus, Bithynia, Paphlagonia and Pontus.

During the Greek wars with Persia, in August 480 BC, as recounted in Book VIII of Herodotus' "Histories", Athens was evacuated (VIII.41; Rawlinson, 1996, pp. 628–629) before Xerxes' Persians arrived and sacked

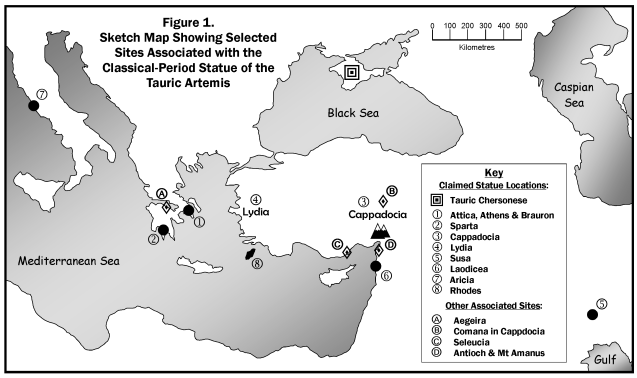


*Figure 1* – Sketch map showing selected sites associated with the classical-period statue of the Tauric Artemis.

the city (VIII.50–53; op. cit., pp. 631–632). Pausanias, in support of his preferred alternate explanation, expressed astonishment that if it were the original, the Athenians apparently failed to take the Tauric Artemis with them ("Description of Greece" Book III, XVI.7; Jones & Ormerod, 1926, pp. 100–101). He repeated the belief that as they did not, it was taken as booty by the Persians back to Susa, north of the Gulf. Seleucus I (312–281 BC), who later controlled a large part of the former Persian Empire, was said to have given the statue to the Laodiceans, who still claimed to possess it in Pausanias' day (Book III, XVI.8–9; loc. cit.).

Frazer's (1921) Footnote 2 on pp. 275–276 of his translation of Apollodorus' "Epitome", referred to the later ancient/early medieval writers, who suggested Orestes and Iphigenia had taken the image concealed in a bundle of faggots to Aricia in Italy, rather than back to Greece, or who had indicated Orestes had left images of Artemis in numerous places. Such tales may simply reflect the later continued growth of the legendary surrounding the statue, and the multiplication of sites claiming it. Even in Apollodorus' time ("Epitome", VI.27–28; op. cit., pp. 274–277), he was able to record a further variant where Orestes was said to have been driven onto the island of Rhodes in a storm, where an oracle instructed him to dedicate the image into the wall of a fortification, something found in no other ancient text.

More legends survived of places Iphigenia and/or Orestes were believed to have visited, and left their mark, but not the statue. At Aegeira by the southern shore of the Gulf of Corinth in southern Greece, Pausanias ("Description of Greece" Book VII, XXVI.5; Jones, 1933, pp. 330–331) remarked on a temple to Artemis with a modern image, as well as an ancient image said to have been of Iphigenia, which led him to suggest the temple must originally have been dedicated to her, not Artemis. Frazer (1921, Footnote 1, p. 277) listed the unknown island of Sminthe Orestes and Iphigenia were said to have landed on when coming home, as well as the landlocked site of Comana in Cappadocia, where Orestes supposedly instituted the worship of Artemis Tauropolus. The medieval Tzetzes brothers' commentaries on ancient authors added that Orestes was forced by storms to the northeast angle of the Mediterranean, and he landed in the regions where Seleucia and Antioch were later built. Nearby Mount Amanus, long known for its metal mines back into the 3rd millennium BC, was said to have been named as it was the place where he was freed of his madness. This revolved around the dubious derivation of 'Amanus' from the Greek 'mania' (= 'madness'), however. Orestes' link to Comana seemed to have relied on an equally questionable etymology alone.

## 5 Conclusion

There are certain similarities in the 'barbarous' blood-rituals associated with the Tauric Artemis and the Magna Mater stone from Pessinus in west-central modern Turkey, that we discussed previously, but quite what about the Iphigenia-Orestes story led to its assuming so widespread a significance anciently is not certain. That their tales linked to Greece with Greek characters might account for the reduplication of Tauric Artemis' statues there, but it is less obvious why this interest should have spread to so many other places. What is clearer is the central importance of an object believed to have fallen from the sky in all this.

## References

Frazer J. G. (1921). *Apollodorus, The Library, Volume II.* Harvard University Press (Loeb Classical Library imprint).

Graves R. (1992). *The Greek Myths: Combined Edition.* Penguin Books.

Jones W. H. S. (1918). *Pausanias: Description of Greece I - Books I and II.* Harvard University Press & William Heinemann (Loeb Classical Library imprint).

Jones W. H. S. (1933). *Pausanias: Description of Greece III - Books VI–VIII.* Harvard University Press & William Heinemann (Loeb Classical Library imprint).

Jones W. H. S. and Ormerod H. A. (1926). *Pausanias: Description of Greece II - Books III–V.* Harvard University Press & William Heinemann (Loeb Classical Library imprint).

McBeath A. and Gheorghe A. D. (2004). "Meteor beliefs project: The palladium in ancient and early medieval sources". *WGN*, **32:4**, 117–121.

McBeath A. and Gheorghe A. D. (2005). "Meteor beliefs project: Meteorite worship in the ancient greek and roman worlds". *WGN*, **33:5**, 135–144.

Rawlinson G. (1996). *Herodotus: Histories.* Wordsworth Classics.

Way A. S. (1912). *Euripides in Four Volumes: II - Electra, Orestes, Iphigeneia in Taurica, Andromache, Cyclops.* William Heinemann & Harvard University Press (Loeb Classical Library imprint).

*Handling Editor:* Javor Kac

This paper has been typeset from a LaTeX file prepared by the author.

# The International Meteor Organization

web site http://www.imo.net

## Council

*President:* Jürgen Rendtel,
Eschenweg 16, D-14476 Marquardt, Germany.
tel. +49 33208 50753
e-mail: jrendtel@aip.de

*Vice-President* Alastair McBeath
12A Prior's Walk, Morpeth,
Northumberland NE61 2RF, UK.
tel. +44 1670 518487
e-mail: meteor@popastro.com

*Secretary-General:* Robert Lunsford
1828 Cobblecreek Street, Chula Vista,
CA 91913-3917, USA. tel. +1 619 585 9642
e-mail: lunro.imo.usa@cox.net

*Treasurer:* Marc Gyssens, Heerbaan 74,
B-2530 Boechout, Belgium.
e-mail: marc.gyssens@uhasselt.be
BIC: GEBABEBB
IBAN: BE30 0014 7327 5911
Always state BIC and IBAN codes together!
Check international transfer charges with your bank; you are responsible for paying these.

*Other Council members:*

Rainer Arlt, Friedenstraße 5, D-14109 Berlin, Germany. e-mail: rarlt@aip.de

David Asher, Armagh Observatory, College Hill, Armagh BT61 9DG, Northern Ireland, UK;
e-mail: dja@star.arm.ac.uk

Huan Meng, 262, 23 Qun Fang Si Yuan, Tongzhou District, Beijing 101121, China
e-mail: hmeng@bjp.org.cn

Sirko Molau, Abenstalstraße 13b, D-84072 Seysdorf, Germany.
e-mail: sirko@molau.de

Chris Trayner, 32 Moor Park Villas, Leeds LS6 4BZ, UK
e-mail: c.trayner@leeds.ac.uk

Mihaela Triglav-Čekada, Streliška 9, SI–1000 Ljubljana, Slovenia.
e-mail: mtriglav@yahoo.com

Josep Trigo-Rodriguez, Inst. Estud. Espacials de Catalunya, Campus UAB, Facultat de Ciencies, 08193 Bellaterra (Barcelona), Spain.
e-mail: trigo@ieec.uab.es

Cis Verbeeck, Grote Steenweg 469, 2600 Berchem, Belgium. tel. +32 3 239 00 80
e-mail: cis.verbeeck@scarlet.be

## Commission Directors

*FIreball DAta Center:* André Knöfel
Am Observatorium 2,
D-15848 Lindenberg, Germany.
e-mail: fidac@imo.net

*Photographic Commission:* vacant

*Radio Commission:* Jean-Louis Rault
Société Astronomique de France,
16, rue de la Vallée, 91360 Epinay sur Orge, France
email: f6agr@orange.fr

*Telescopic Commission:* Malcolm Currie
25, Collett Way, Grove,
Wantage, Oxfordshire OX12 0NT, UK.
e-mail: mjc@star.rl.ac.uk

*Video Commission:* Sirko Molau

*Visual Commission:* Rainer Arlt

# WGN

*Editor-in-chief:* Javor Kac
Na Ajdov hrib 24, SI-2310 Slovenska Bistrica, Slovenia. e-mail: wgn@imo.net;
include METEOR in the e-mail subject line

*Editorial board:* Ž. Andreić, R. Arlt, D.J. Asher, J. Correira, M. Gyssens, H.V. Hendrix, C. Hergenrother, J. Rendtel, J.-L. Rault, C. Trayner, M. Triglav-Čekada, C. Verbeeck.

*Advisory board:* M. Beech, P. Brown, M. Currie, M. de Lignie, W.G. Elford, R.L. Hawkes, D.W. Hughes, J. Jones, C. Keay, G.W. Kronk, R.H. McNaught, P. Pravec, G. Spalding, M. Šimek, I. Williams.

# IMO Sales

| *Available from the Treasurer or the Electronic Shop on the IMO Website* | € | $ |
|---|---|---|
| **IMO membership, including subscription to WGN Vol. 37 (2009)** | | |
| Surface mail | 26 | 36 |
| Air Mail (outside Europe only) | 49 | 69 |
| **Back issues of WGN** on paper | | |
| Vols. 26 (1998) – 36 (2008) except 30 (2002), per complete volume | 15 | 21 |
| **Proceedings of the International Meteor Conference** on paper | | |
| 1990, 1991, 1993, 1995, 1996, 1999, 2000, 2002, 2003, 2004, per year | 10 | 14 |
| 2005, 2006 | 15 | 21 |
| **Proceedings of the Meteor Orbit Determination Workshop 2006** | 15 | 21 |
| **Proceedings of the Radio Meteor School** on paper | | |
| 2005 *(Reprinted — available again)* | 15 | 21 |
| **Electronic media** | | |
| DVD: WGN Vols. 6–30 & IMC 1991, 1993–96, 2001–04 | 45 | 63 |

# Radiant plots of the IMO Video Meteor Network

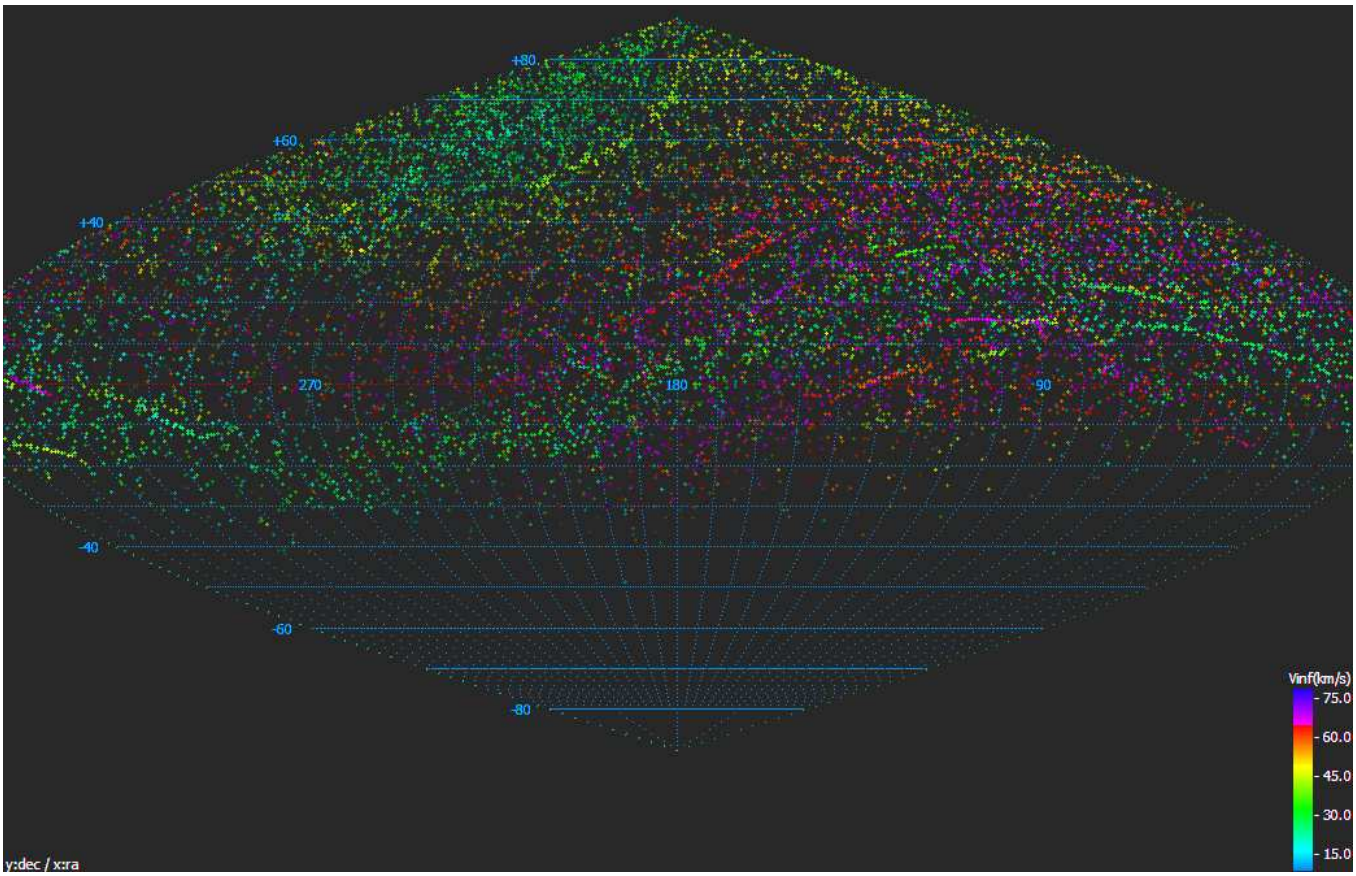


Distribution of radiants detected in the IMO Video Meteor Database over right ascension and declination in a sinusoidal projection. The brightness of each spot represents the number of meteors that contributed to the radiant, and the meteor shower velocity is coded in the color.

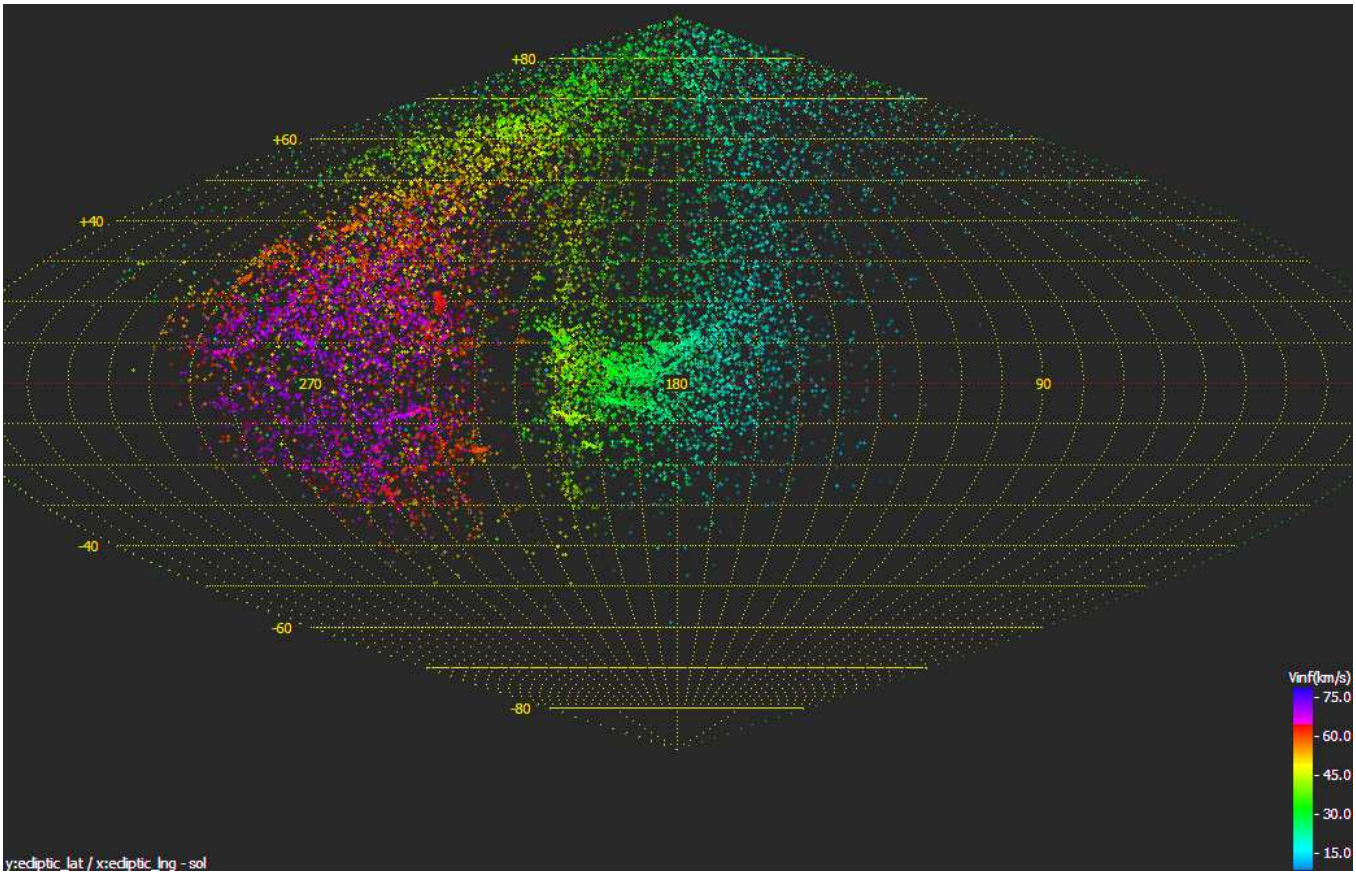


Distribution of radiants detected in the IMO Video Meteor Database in Sun-centered ecliptical coordinates with the ecliptical radiant longitude minus the solar longitude as x-axis, and the ecliptical latitude as y-axis. For more information and full analysis of the IMO Video Meteor Network data, see the paper by Molau and Rendtel on page 98.